Thesis Report

Electrochemical Dicarboxylation of 1,3-butadiene with Captured CO_2 to Produce 3-hexene-1,6-dioic acid, a Precursor to Adipic Acid

Adwait Bhingarde

Delft University of Technology

TU Delft

Thesis Report

Electrochemical Dicarboxylation of 1,3-butadiene with Captured CO_2 to Produce 3-hexene-1,6-dioic acid, a Precursor to Adipic Acid

by

Adwait Bhingarde

Thesis supervisor:	Prof. Dr. Wiebren de Jong
Daily supervisor:	Dr. Ruud Kortlever
Daily co-supervisor:	Dr. Shahid Khan
Project Duration:	December 2024 - July 2025
Faculty:	Faculty of Mechanical Engineering, Delft

TU Delft

Preface

This thesis marks the culmination of my academic journey at Delft University of Technology. Reflecting on this experience has been deeply enriching, academically and personally. I am beyond grateful to have had the opportunity to research electrochemistry for climate-conscious innovation with one of the world's premier research groups.

Tackling the climate change crisis and an ambition to provide clean energy to everyone is paramount to me, and the ability to contribute to it in the most fundamental manner is absolutely rewarding. This would not have been possible without the unwavering support and guidance of my thesis supervisor, Prof. Dr. Ir. Wiebren de Jong. I am grateful for the pragmatic insights and niche knowledge transfer from Dr. Ruud Kortlever, which greatly strengthened the foundation of this thesis. My gratitude also extends to Dr. Shahid Khan for allowing me to fail, explore and learn, alongside equipping me with a panoply of laboratory skills for research. Lastly, I thank Michel van den Brink, the brilliant minds from the Kortlever Research Group, and my lab peers for adding valuable depth to this project.

To my parents, who have been the wind beneath my wings, thank you for being my biggest cheerleaders through thick and thin; this degree is as much yours as it is mine. Your belief in me has been truly unparalleled. I would also like to thank my family and dearest friends from Mumbai, Delft and across the world who have contributed to maintaining my sanity throughout these rigorous two years.

I ventured into this master's program with a vision to excel, and this thesis has allowed me to push my limits by a margin. I carry forward immense confidence and strength as I prepare to step into the industrial world full of opportunities. With an aim to steer change in the renewable energy sector, I hope to return to my alma mater one day with knowledge, experience and purpose. The rollercoaster ride at Delft University of Technology will be cherished forever.

Adwait Bhingarde
Delft, July 2025

Abstract

The current global average CO_2 concentration in the air is 427 ppm, rising at a rate of 2 ppm per year, faster than ever before. This underscores the urgency to capture and either utilise or sequester the carbon. The energy transition is driving a shift from fossil-based generation towards renewable energy sources, with wind and solar energy generation at the forefront. The intermittency of supply from renewable energy generation presents opportunities during peak electricity generation to reduce CO_2 electrochemically.

The electrochemical utilisation of captured CO_2 offers a sustainable pathway to close the carbon loop by converting waste carbon into value-added chemicals. This thesis explores the electrochemical dicarboxylation of 1,3-butadiene with CO_2 to produce 3-hexene-1,6-dioic acid (3HDA), a direct precursor to adipic acid. Adipic acid is a key raw material in Nylon-66 production, and its conventional synthesis from cyclohexane emits significant quantities of N_2O, a greenhouse gas with a global warming potential of 298 times that of CO_2. In contrast, the pathway studied here aims to decarbonise the process using renewable electricity and non-fossil carbon inputs.

The electrochemical synthesis of 3HDA from 1,3-butadiene and CO_2 is employed in an electrolyser cell. Using a sealed, undivided electrochemical cell with acetonitrile and tetraethylammonium chloride as the electrolyte solution, the study systematically investigates the influence of various electrocatalyst morphologies and materials, and process parameters on faradaic efficiency, product selectivity and yield.

Nickel wire was identified as the most effective working electrode, outperforming copper wire and other nickel-based morphologies, employed alongside aluminium coil as a sacrificial anode. Electrochemical characterisation using cyclic voltammetry and chronoamperometry revealed –2.6 V vs Ag/AgCl as the optimal potential for 3HDA formation, with a faradaic efficiency achieved of 14% for 3HDA and 100% selectivity among the carboxylated products. Competing side reactions, such as 3-pentenoic acid (3PA), formate and oxalic acid production, were observed at other reduction potentials. Reduced moisture content in the electrolyte was found to poorly influence the faradaic efficiency. The dry acetonitrile has a similar 3HDA faradaic efficiency when the water content is reduced from 350 ppm to 150 ppm in the electrolyte. Temperature studies indicated that higher temperatures enhance the reaction rate but increase product solubility, reducing solid product formation. Solubility measurements confirmed this behaviour. On calculating the faradaic efficiency of the dissolved 3HDA as well, the efficiency stands at 6.58% for at 40°C and 3.59% at 60°C. Further, experimentation with alternative supporting electrolytes like $TBABF_4$ and $TBAPF_6$ was inconclusive due to practical limitations.

Overall, the thesis demonstrates a promising proof-of-concept for the sustainable electrochemical conversion of CO_2 and 1,3-butadiene to value-added chemicals of adipic acid. The findings contribute to the broader goals of electrifying chemical synthesis and valorising captured CO_2, inspiring future work recommended in improving the process conditions and refining electrolyte and electrode design.

Contents

List of Figures

List of Tables

Nomenclature

Abbreviations	Description
CO_2	Carbon Dioxide
3HDA	3-hexene-1,6-dioic acid
3PA	3-pentenoic acid
HPLC	High Performance Liquid Chromatography
GC	Gas Chromatography
LGC	Liquid Gas Chromatography
CV	Cyclic Voltammetry
CA	Chronoamperometry
CP	Chronopotentiometry
HER	Hydrogen Evolution Reaction
ECSA	Electrochemical Surface Area
Ni	Nickel
Cu	Copper
ACN/MeCN	Acetonitrile
TEACl	Tetraethylammonium Chloride
$TBABF_4$	Tetrabutylammonium tetrafluoroborate
$TBAPF_6$	Tetrabutylammonium hexafluorophosphate
DMF	Dimethylformamide
DMSO	Dimethyl sulfoxide
CEM	Cation Exchange Membrane
SCE	Standard Calomel Electrode
Ag/AgCl	Silver/Silver Chloride
GC-TCD	Gas Chromatograph with Thermal Conductivity Detector
GC-FID	Gas Chromatograph with Flame Ionisation Detector
DAD	Diode Array Detector
LC-MS	Liquid Chromatography–Mass Spectrometry
SOP	Standard Operating Procedure
SEM	Scanning Electron Microscopy
ppm	Parts Per Million
MPa	Megapascal
$mA.cm^{-2}$	Milliampere per square centimetre
°C	Degrees Celsius
mS/cm	Millisiemens per centimetre
FE	Faradaic Efficiency
GWP	Global Warming Potential
N_2O	Nitrous Oxide

CO	Carbon Monoxide
OA	Oxalic Acid
NaOH	Sodium Hydroxide
H_2SO_4	Sulphuric Acid
CV (plot)	Cyclic Voltammogram
CO_2RR	Carbon Dioxide Reduction Reaction

1

Introduction

Rising CO_2 concentration in the environment has been of great concern in recent decades, with the increase in CO_2 levels by almost 2ppm yearly, which accounts for a yearly growth of almost 0.5%. Currently, the global average CO_2 concentration is at 427 ppm [22]. This measures for storage and utilisation opportunities for CO_2 in the fossil fuel-dominated industry and the energy transition being underway to achieve the goal of zero carbon emissions by 2050. Currently, only 1 % of the anthropogenic CO_2 emissions is utilised to recycle back into the system.

As the blue fuel alternatives are becoming a popular choice to allow a smooth transition to renewable energy systems, research in Carbon Capture and Storage (CCS) and Carbon Capture and Utilisation (CCU) is at the centre of discussion and research. These technologies recycle the CO_2 back into the system and reduce the effective carbon footprint. CO_2 can be converted to several high-value chain chemical products, including polymers and hydrocarbons, and sustainable fuels, which are pivotal for the maritime and aviation industries. Recently, some petrol mixtures utilise bio-ethanol synthesised from captured CO_2 for roadway transportation. While CO_2 can be reduced photochemically and electrochemically, the electrochemical reduction of CO_2 is gaining attention to utilise the peak electricity generated due to the intermittency of renewable energy sources like wind and solar power. The increasing interest in electrochemical CO_2 reduction has led to significant research into integrating CO_2 with organic reactants to synthesise functionalized products. One such promising approach is the electroreduction of CO_2 with 1,3-butadiene, which synthesises 3-hexene-1,6-dioic acid (3HDA) [6], an essential precursor in the synthesis of adipic acid, responsible for 90% of Nylon 66 production [8].

Today, the global Adipic Acid production is 2.5 million tonnes per year, taking a massive share in industrial processes [32]. The traditional process for making adipic acid has been using Nitric Acid (HNO3) for the oxidation of the mixture of cyclohexane and cyclohexanone called KA oil [40], which generates significant N_2O emissions, a potent greenhouse gas. 300 grams of N_2O are emitted per kilogram of Adipic Acid produced [18]. The Global Warming Potential (GWP) of N_2O is 298 times that of CO_2, making the emissions 89.4 kg of CO_2e per kg of adipic acid produced [1]. This expresses the urgency to decarbonise such a major industrial process.

The primary advantage of electrochemical CO_2 reduction lies in its ability to directly convert CO_2 into valuable products under mild reaction conditions using renewable electricity. However, optimising the fardaic efficiency and product selectivity in the CO_2-1,3-butadiene coupling process requires a comprehensive understanding of reaction mechanisms, electrocatalyst materials, electrolyte compositions, and reactor configurations. Recent advancements in electrocarboxylation include the development of catalysts, redox mediators, and continuous flow electrochemical cells. Concerning the electrochemical dicarboxylation of 1,3-butadiene with CO_2, the reaction is performed at a higher pressure inlet of CO_2. In this setup, the side products, like the monocarboxylated product 3-pentenoic acid, is also prominent

in the product distribution. Additionally, the electrocatalyst tested for efficient production of 3HDA is not explicitly mentioned in terms of its morphologies. These research gaps are mentioned in detail in Chapter 2, but serve as a basis to design the research questions.

The thesis aims to answer the following research questions in detail, supported by the sub-research questions:

Main research question: What are the optimised reaction materials, parameters and conditions for the low-pressure CO_2 reduction with 1,3-butadiene in the synthesis of 3-hexene-1,6-dioic acid?

1. What are the impacts of different electrode materials and electrode morphology on product selectivity and faradaic efficiency of 3HDA?

2. What are the side products formed during the electrochemical reduction of CO_2 and 1,3-butadiene, and how do they affect the efficiency of 3HDA production?

3. How does the moisture in the electrolyte affect the production of 3HDA, and what are the measures for optimisation?

4. How do varying reaction conditions impact the faradaic efficiency in the synthesis of 3HDA?

In order to develop fulfilling answers to these questions, the report proceeds via a detailed literature study, a developed experimental method, results and discussion, and conclusion and recommendations for future research. The report raises questions and develops areas for improvement, and later provides results to prove the hypothesis. This thesis is an experimental attempt at creating a better and efficient process for 3HDA production in a CO_2 electrolyser. The following Chapter 2, provides a brief overview of the process and reaction mechanism and how it builds the foundation for the research of this thesis. It explores the research gaps in detail and inspires strategies for experimental methodology, which is mentioned in Chapter 3. In the experimental methodology, the electrochemical techniques for product synthesis and the analytical techniques for accurately quantifying the products to determine the output parameters are mentioned. This methodology is followed for research in the laboratory, and the results of the experiments are mentioned in Chapter 4. The results are supported by in-depth discussions and analyses, which lead to constructive conclusions mentioned in Chapter 5. Finally, the shortcomings of the thesis are given an outlook for future research that may improve the faradaic efficiency of 3HDA in Chapter 6.

2

Literature

This chapter aims to provide a comprehensive overview of the development of the process to understand the redox mechanism for electrodicarboxylation synthesis. It further focuses on exploring the choice of electrocatalysts, electrolyte solvents and supporting electrolytes, cell design and parameters like pressure, which influence selectivity, faradaic efficiency and yield of the desired and undesired products formed. Finally, a patented state-of-the-art process is studied to inspire the research and to aid reasoning for the analysis in the forthcoming chapters.

2.1. Process Development

To understand how a process is developed, modified, and integrated, it is important to understand how a process began as a part of the mainstream production unit. Adipic Acid production began with the process of oxidation of cyclohexane in 1906, when French chemists Bouveault and Locquin reported the synthesis methodology. Today, the global Adipic Acid production is 2.5 million tonnes per year, taking a massive share in industrial processes [32]. The traditional process for making adipic acid has been using Nitric Acid (HNO3) for the oxidation of the mixture of cyclohexane and cyclohexanone called KA oil [40], which generates significant N_2O emissions, a potent greenhouse gas. 300 grams of N_2O are emitted per kilogram of Adipic Acid produced [18]. The Global Warming Potential (GWP) of N_2O is 298 times that of CO_2, making the emissions 89.4 kg of CO_2e per kg of adipic acid produced [1]. The reaction has very low selectivity for cyclohexane in the first step, and thus, a lot of cyclohexane needs to be recycled back into the reactor, adding complexity to the process and making it energy-intensive. Additionally, due to the reaction conditions' requirement of higher temperatures (about $130°C$) and excessive N_2O emission, which is harmful to the environment, alternatives are investigated for the oxidation of cyclohexane and cyclohexanone. Using oxygen from the air and hydrogen peroxide for the oxidation of cyclohexane, cyclohexanone and n-hexane is reviewed by Stijn Van de Vyver et. al [38]. However, the processes aren't developed to an extent where the catalysts are efficient and have a scope of competing with the existing process.

The traditional processes focused on the oxidation of cyclohexane and cyclohexanone to make adipic acid, and the demerits are as mentioned above. Among other process pathways is the biocatalytic conversion of vegetable oil or α-ketoglutaric acid and the dicarboxylation of 1,3-butadiene or 1,4-methoxy-2-butene [38]. Significant modern-day research efforts and advancements in producing adipic acid from 1,3-butadiene by a two-step electrochemical carboxylation process make it favourable to base the research area on. 1,3-butadiene when electrochemically reduced with CO_2, produces 3-hexenedioic acid, a 1,4-addition product, as the main product and 2-ethenyl-succinic acid and 3-pentenoic acid as product of monocarboxylation [6]. The plausible mechanism of the reaction and kinetics are discussed in depth in the forthcoming section.

2.2. Mechanism

CO_2 is thermodynamically very stable, making its reduction relatively difficult, with $\Delta G_f^0 = -396kJ/mol$ [24]. CO_2 is usually preferred to be reduced electrochemically by applying a suitable potential. In the electrochemical cell, CO_2 is reduced to $CO_2^{\cdot -}$ radical anion by cathodic activation. The radical anion is formed at a potential of -2.21 V vs Standard Calomel Electrode (SCE), i.e. the reference electrode [6].

$$CO_2(g) + e^- \rightarrow CO_2^{\cdot -}, E_o = -2.21V$$

According to Bringmann et al., the reaction is initiated by reducing CO_2 to $CO_2^{\cdot -}$ radical anion at the cathode or working electrode. The $CO_2^{\cdot -}$ radical anion then attacks 1,3-butadiene. The primary reduction of CO_2 is because the recorded 1,3-butadiene reduction potential is -2.6V vs SCE [6]. The $CO_2^{\cdot -}$ radical anion shows C-centred behaviour in an environment where metal or ammonium cations are counterions. In the case of protons being the counterions, $CO_2^{\cdot -}$ radical anions tend to form formic acid [15].

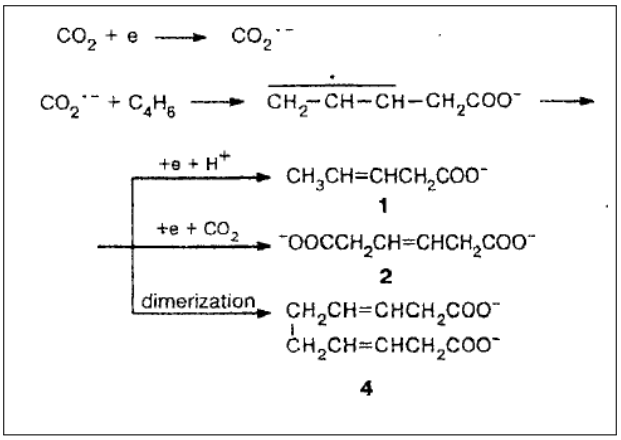

Figure 2.1: Main reaction between CO_2 and 1,3-butadiene to produce 3-hexene-1,6-dioic acid [15]

As observed in Figure 2.1, the product (2) formed is 3-hexene-1,6-dioic acid, primarily from the double nucleophilic substitution attack of $CO_2^{\cdot -}$ radical anion on 1,3-butadiene. The product (1) formed is reported in Figure 2.1 is 3-pentenoic acid, formed by the monocarboxylation of 1,3-butadiene. The typical anode side reactions that follow in the electrochemical cell are as mentioned below. Examples of Aluminium and Magnesium are taken as they are the popular sacrificial anodes used in industrially scalable electrochemical synthesis [15].

$$Al \rightarrow Al^{3+} + 3e^-$$
$$Mg \rightarrow Mg^{2+} + 2e^-$$
$$H_2O \rightarrow 2H^+ + \frac{1}{2}O_2 + 2e^-$$
$$H_2 \rightarrow 2H^+ + 2e^-$$

The preferred product of 3HDA, called as C6 product, is formed by the 1,4-addition pathway, that is, the addition of $CO_2^{\cdot -}$ radical anion to the 1st and 4th carbon atom in 1,3-butadiene. As seen in Figure 2.2, the product (4) is 3-HDA. It is formed by the initial attack of $CO_2^{\cdot -}$ radical anion on the 1st carbon of 1,3-butadiene, forming an intermediate where the charge is localised on the second and the fourth carbon atom. Both these molecules are in equilibrium. The second $CO_2^{\cdot -}$ radical anion fixation on the second carbon leads to the formation of product (3) from Figure 2.2 i.e. 1,2-(2-ethenyl-succinic acid), and the second $CO_2^{\cdot -}$ radical anion fixation on the fourth carbon leads to the formation of product (4), i.e

3HDA. Since these products can be formed interchangeably in quantities upon the 2-step carboxylation of 1,3-butadiene, there are various factors like the electrolyte composition, electrocatalyst, mediators, cell design and pressure-temperature conditions that influence the production of the preferred C6 product, which will be discussed in the successive sections.

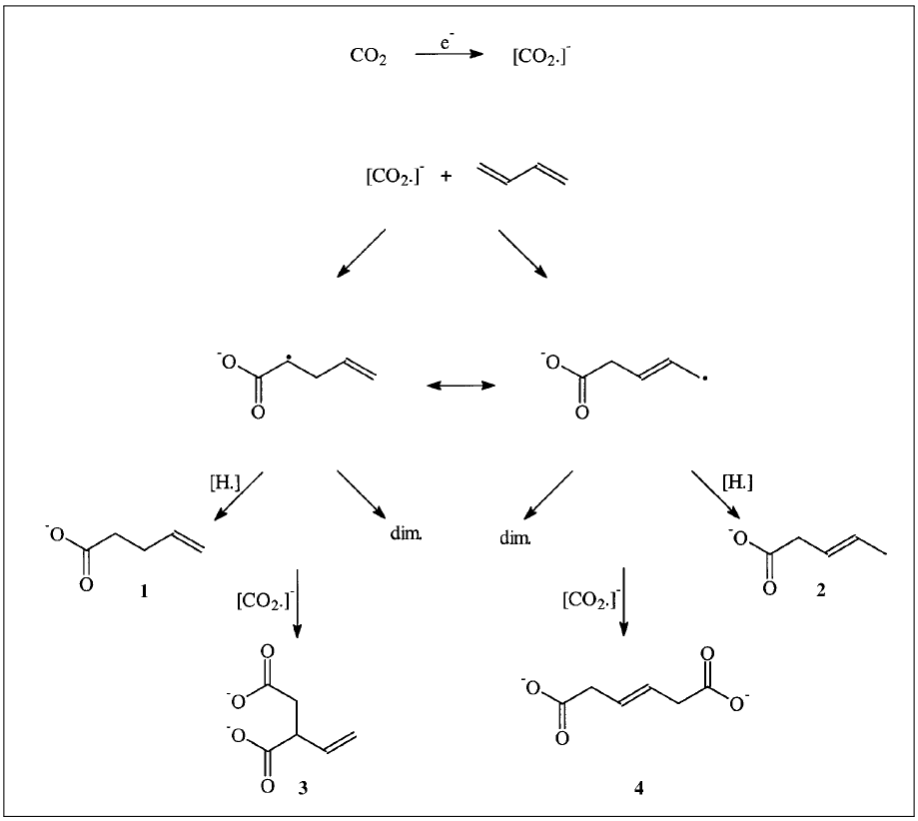

Figure 2.2: Reaction mechanism following the attack of $CO_2^{\cdot -}$ radical anion on 1,3-butadiene [6]

There is another favoured pathway [23] which states that 1,3-butadiene and CO_2 are simultaneously reduced at the working electrode and the reaction proceeds by nucleophilic attack of the butadiene radical anion on CO_2 and $CO_2^{\cdot -}$ radical anion on 1,3-butadiene. As seen in Figure 2.3, the reduction current of 1,3-butadiene and CO_2 is similar at approximately -2.25 V reduction potential vs SCE [23]. This lays the foundation for another plausible mechanism of simultaneous reduction of the reactants at the working electrode under the same conditions.

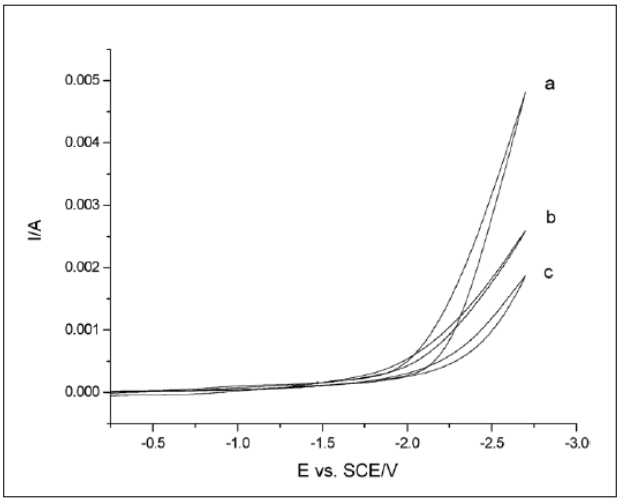

Figure 2.3: Cyclic Voltammograms of (a) only addition of 1,3-butadiene in electrolyte, (b) simultaneous presence of 1,3-butadiene and saturated $CO2$ in the electrolyte, and (c) only saturation of the electrolyte with CO_2 [23]

A mechanism that suggests the simultaneous reduction of CO_2 and 1,3-butadiene can be seen from Figure 2.4. The intermediate A is formed by the nucleophilic attack of the CO_2^- radical anion on 1,3-butadiene and the butadiene radical anion attack on CO_2. This intermediate A is in equilibrium with the intermediate B, which is a steric isomer. On further attack of CO_2^- radical anion on the intermediates A and B, cis and trans 3HDA are formed as products. In the dicarboxylation of other conjugated dienes which have substituted groups, only the trans isomer of the dicarboxylated product is formed. The dependence of cis and trans products formed depends on the electrocatalyst used. The ratio of cis and trans-3-HDA formed as per the second mechanism is 1:1 [23]. As per the electrocarboxylation review by Matthessen et al., the cis-configured product is more reactive and has a greater effect on the rate of dicarboxylation [24]. The cis product has a lower boiling point than the trans product and thus elutes faster, and the cis peak is observed before the trans product peak in High Performance Liquid Chromatography (HPLC) analysis [6]. Although in a later event, the 3HDA product is synthesised with a view of converting it to adipic acid, and both the cis and the trans isomers are converted to adipic acid by one step of hydrogenation.

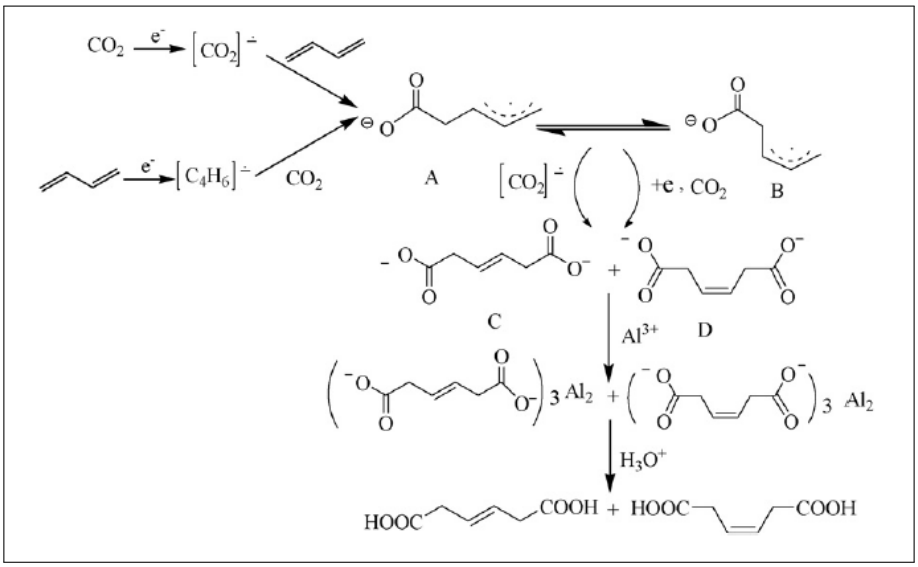

Figure 2.4: Reaction mechanism following the attack of CO_2^- radical anion and 1,3-butadiene radical anion simultaneously [23]

2.3. Electrocatalyst and Electrolyte

The electrocatalyst and the electrolyte used for the reaction affect the selectivity, yield, and faradaic efficiency of the process as they may alter the mechanism pathways and kinetics. To understand the drive that allows optimisation on the foreground of the cell components, firstly, it is essential to understand the reactions occurring at the anode and cathode and the process of the reaction pathway.

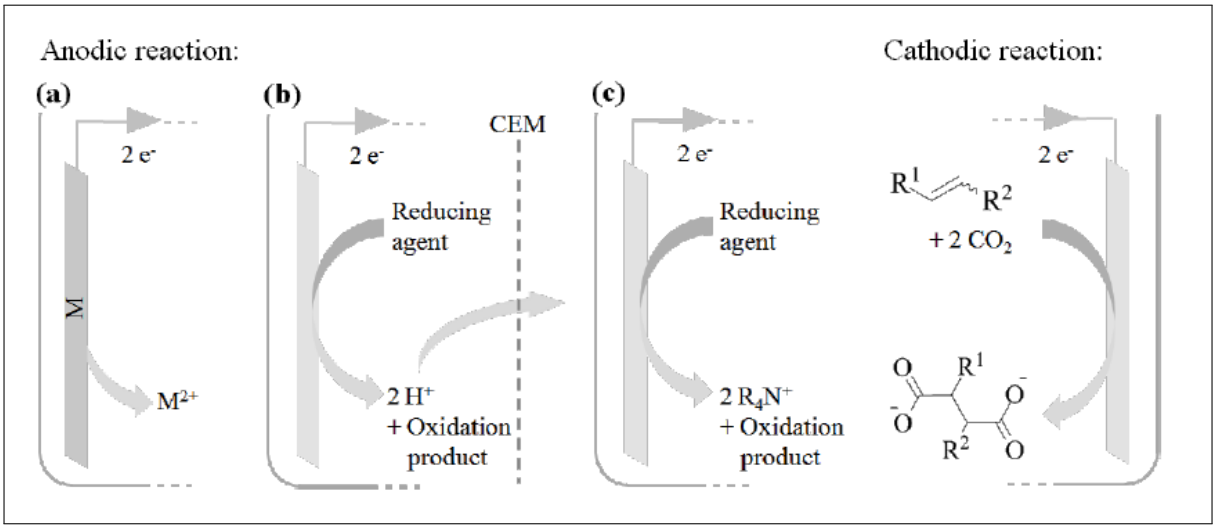

Figure 2.5: Electrocarboxylation steps in the cell and reactions at anode and cathode [24]

Sacrificial or non-sacrificial anodes are used based on the process conditions and the reaction mechanisms. In Figure 2.5, a sacrificial anode is taken into consideration in subfigure (a), an inert or non-sacrificial anode is considered in subfigure (b), and a cation exchange membrane is used for separating the catholyte and the anolyte. Tetraalkylammonium salts are commonly used with organic electrolyte solvents. The reducing agent or the sacrificial anode is oxidised at the anode and CO_2 and 1,3-butadiene is reduced at the cathode. The oxidised agents at the anode combine with the intermediates of the first step of carboxylation and provide them with the required conductivity in the bulk phase to be present near the cathode to be reduced by the CO_2^{-} radical anion for the 1,4-addition product. These anodes, due to their higher oxidation potential compared to other reaction species, allow for efficient reactions in undivided cells, eliminating the need for a membrane between the catholyte and anolyte [23].

Popular choices of sacrificial anodes are Magnesium and Aluminium, and for inert anodes are Platinum or Carbon [24]. The use of sacrificial anodes in electrochemical CO_2 fixation systems offers several advantages, such as enabling high current densities at relatively low potentials, which minimises energy consumption. The oxidation of sacrificial anodes delivers metal cations like Mg^{2+} or Al^{3+} which coordinate with the carboxylate anions formed at the cathode, facilitating the formation of metal carboxylates that can easily be precipitated from organic solvents for product isolation. However, the gradual consumption of the anode material presents a significant drawback for industrial applications, as the metal consumption can be expensive and limits continuous processing. This makes sacrificial anode-based systems more suitable for fine chemical applications, where the carboxylate salt can be used directly [24].

Replacing the sacrificial anode with an inert anode introduces several challenges, including the need for a counter-electrode reaction that delivers cations to balance the carboxylate anions. The anodic reaction must involve a species that is more easily oxidised than others in the reaction mixture, and any byproducts should either not interfere with the system or contribute beneficially to the cathodic reaction. One of the challenges with using inert anodes is the potential formation of protons at the anode, which

can negatively affect the efficiency of the electrocarboxylation by promoting side reactions, such as hydrogen or formic acid formation at the cathode. To minimise such side reactions, cathode materials with high hydrogen overvoltage, such as lead, mercury, tantalum, or zinc, can be used [24].

An alternative approach involves the anodic oxidation of tetraalkylammonium salts, which function as counter cations for the cathodic carboxylate anions. Although this method is similar to sacrificial anodes, it is better suited for continuous processes and avoids the challenges associated with dissolving metal anodes. However, the tetraalkylammonium salts are consumed during the reaction, which can also be considered a sacrificial process because of the salts getting consumed [24].

Cathode or working electrode selection for the electrochemical process is very crucial. As known from the section 2.2, the reaction can proceed via two mechanistic pathways. Hence, the absorption of CO_2 and 1,3-butadiene at the cathode surface needs preference. As seen in the Table 2.1, different cathode materials are studied for a better yield and efficiency of 3HDA product. Isolated yield is the yield of the desired product based on a collection and separation basis compared to the amount of 1,3-butadiene present before the reaction. The electrochemical cell conditions were at room temperature, 3 MPa pressure, Aluminium (sacrificial) anode, 1,3-butadiene in DMF electrolyte and tetrabutylammonium bromide salt.

Table 2.1: Table for cathode material comparison yielding 3-HDA [23], d: faradaic efficiency

Sr. no.	Cathode material	Isolated Yield (%)	η(%)[d]
1	Ag	5	2.5
2	Zn	10	5
3	Pt	22	11
4	Cu	59	29.5
5	Stainless steel	71	35.5
6	Ni	84	42

It is inferred that Nickel is a better performing cathode material for dicarboxylation in organic solvents. Nickel and Platinum are the top choices of cathodes in electrocarboxylation reactions. Nickel is a favourite catalyst for dienes, especially 1,3-butadiene, as it yields better than Platinum by a margin of approximately 60%. The higher yield generated by employing a Nickel cathode compared to a Platinum cathode is explainable by the logic of carboxylation being affected by the surface morphology over Ni than Pt electrode, or the competing reactions over Pt causing more hindrance than those over Ni [33]. The thermodynamics of the adsorption and carboxylation steps of ethene on Pt closely follow the results observed for Ni, with one key difference being the initial two steps, where CO_2 adsorption on Pt is notably more exothermic than CO_2 chemisorption on Ni. While the second carboxylation step is marginally less exothermic on Pt compared to Ni, this does not affect the overall predicted activity, which primarily depends on the first, endothermic carboxylation step. Therefore, from a thermodynamic perspective, the difficulty of the reaction is similar over both Ni and Pt [33].

To understand the kinetics of the reaction over Ni and Pt catalysts, it is important to know that the first carboxylation is the rate-limiting step [33]. The activation energy for the process on Ni is relatively high, ranging from 1 to 1.2 eV, but still achievable given the approximate handling of the electrochemical environment. In contrast, on Pt, the activation energy required is approximately 0.75 eV higher than on Ni, for the adsoprtion at the surface. This elevated activation energy helps to explain the lower activity of Pt compared to Ni. Additionally, the formation of carbon monoxide and carbonate, which might lead to unnecessary side reactions, occurs more rapidly on Pt than on Ni, as Ni strongly stabilises the atomic oxygen intermediate. This leads to a decrease in the selectivity for carboxylation over Pt [33].

The most commonly used organic solvents are Dimethyl Formamide (DMF), Acetonitrile (ACN) and Dimethyl Sulfoxide (DMSO) because of their adequate oxidation stability and high dielectric constant. The organic solvents are majorly used in the presence of sacrificial anodes as in that case there is no need for an external reducing agent. The organic solvents are aprotic, and hence they need supporting electrolytes to provide mobility and required conductivity in the electrochemical cell. Tetraalkylammonium salts are the favoured supporting electrolytes for the organic aprotic electrolyte solvents. Referring to Table 2.2, the use of different supporting electrolytes affects selectivity and isolated yield. Thus, different supporting electrolytes can be used to check for different required outputs. The data in Table 2.2 is for the electrochemical dicarboxylation of styrene, so it is referred to inspire the study of the effects of different supporting electrolytes [41]. The commonly used supporting electrolytes are Tetrabutylammonium Bromide (TBABr), Tetrabutylammonium Chloride (TBACl), Tetrabutylammonium Iodide (TBAI), Tetraethylammonium Bromide (TEABr), Tetraethylammonium Chloride (TEACl), Tetrabutylammonium hexafluorophosphate (TBAPF6), Tetrabutylammonium tetrafluoroborate (TBABF4), etc. The supporting electrolytes should be used to optimise the process depending on their solubility in the organic electrolyte solvent and its tendency to refrain from participating in any side product formation.

Table 2.2: Supporting electrolytes of Tetraalkylammonium salts in DMF for making arylsuccinic acid from styrene [41]

Sr. no.	Supporting electrolyte	Selectivity of desired product (%)	Isolated Yield (%)
1	TBABr	98	87
2	TBACl	98	74
3	TBAI	90	68
4	TEABr	98	71
5	TMABr	–	–

The review by Matthessen et al., highlights various sacrificial and non-sacrificial anodes, the reducing agents, the use of cation exchange membrane or not, the electrolyte or catholyte-anolyte composition and the carboxylated product distribution ratio between 3-pentenoic acid (C5), 3-hexenedioic acid (C6) and 3-7-decadienedioic acid (C10) with the yield of 3-hexenedioic acid [24].

Table 2.3: Overview of electrodicarboxylation of 1,3-butadiene with CO2 in different process design parameters, h: platinum hydrogen gas diffusion electrode, C5: 3PA, C6: 3HDA, C10: 3,7-decadienedioic acid, f: 1 wt% of H2SO4 solution, d: total current efficiency [24]

Cathode	Anode	Reducing agent	CEM	Solvent (catholyte–anolyte)	C5:C6:C10	η^d (%)	Yield (%)
Hg	Pt	H_2O	Yes	CH_3CN – H_2O^f	67:0:33	18	11
Pb	Pt	dry MgO	Yes	CH_3CN – CH_3CN	26:58:16	31	21
Pb	Pt^h	H_2	No	CH_3CN	0:0:0	0	0
Pb	Pt^h	H_2 + dry MgO	No	CH_3CN	75:25:0	3.7	–
Pb	Pt^h	H_2O	Yes	DMF – H_2O^f	–:–:–	3.4	–
Pb	Pt	NH_3	No	CH_3CN	33:54:13	5.8	–
Carbon felt	Pt	$(TEA)_2$oxalate + TEA formate	No	CH_3CN	36:52:12	39	98
Tantalum	Mg	Anode	No	DMF	2:98:0	–	81
Nickel	Al	Anode	No	DMF	0:100:0	42	84

As observed in Table 2.3, the reducing agent in the case of non-sacrificial anodes is commonly water, dry Magnesium Oxide (MgO), Hydrogen, Ammonia, and Tetraalkylammonium oxalate/formate. In some cases, where non-sacrificial anodes are used in a divided cell configuration, the anolyte is also used as water but is assisted with the use of a cation exchange membrane (CEM) to restrict the hydrogen evolution reaction (HER) which may suppress the formation desired products or favor formation of formic acid and promote C5 and C10 products [24]. MgO and tetraalkylammonium salts are also sacrificial reducing agents for a non-sacrificial anode set-up, which holds value as they allow the process

to be designed for continuous operation.

To conclude, the literature research for electrolytes and electrocatalysts, electrocarboxylation of 1,3-butadiene is not the best in aqueous or protic electrolyte medium. Although MgO is a promising alternative to water, its solubility in organic solvents is limited. Thus, utilising tetraalkylammonium cations increases selectivity for the 3-HDA (C6) product. In organic electrolyte solvents, the best-used are sacrificial anodes to improve the selectivity of the C6 product, and the reference electrodes used are SCE, Ag/AgCl or Ag/AgBr. The environment being aprotic, the use of a working electrode as Nickel, also a catalyst, favours faster $CO2$ reduction to CO_2^- radical anion aiding the first step of carboxylation, which is rate-determining [24]. The use of Nickel as the cathode further debars the use of mediators like iron redox mediators for providing stability by forming organometallic complexes [24].

2.4. Effect of Parameters and Cell Design

As seen in the Table 2.3, when a catholyte-anolyte configuration is used, the cell is supposed to be divided by a cation exchange membrane and in the presence of a common electrolyte, the cell can be undivided. The CEM is used to avoid the supply of protons to the catholyte, to refrain from the formation of formate. If the configuration has mercury or lead cathodes, they ought to form hydrogen gas to minimise current loss due to their high hydrogen overpotential [24].

Since the formation of the C6 product is of prime importance, over the years, organic solvents with tetraalkylammonium supporting electrolytes have gained benefit. This naturally tends towards having a single undivided cell for operation. Additionally, the divided (H cell) cell's CEM is sensitive to organic solvents and needs to be replaced or backcycled after use to maintain the quality of electrolysis. As the capital cost is high and the operation involves complexity by creating a wider inter-electrode gap, putting it into operation often becomes challenging. Thus, the electrolysis for aprotic solvents is best done in a single undivided cell configuration [29].

Another major reason for using undivided cells is that the pressure of CO_2 can be increased to study its effect on the yield and efficiency of the process, as the CEM can be damaged at higher inlet pressure [24]. The analysis by Li et al. provides an experimental result of increasing the pressure of CO_2 in the progression of 1 MPa between the range of 1 MPa to 5 MPa [23]. It is observed that with increasing pressure, the yield of the C6 desired product increases, also increasing the current efficiency at the same time as observed in Table 2.4. Thus, it is safe to mention that the CO_2 solubility increases with an increase in pressure, thus having more CO_2 available for the endothermic reaction rate-controlling step. However, the yield and efficiency remain almost the same between 3 MPa to 5 MPa, suggesting overpotential trigger and carbonates formation beyond a certain pressure [23]. Thus, the inlet pressure between 2 MPa to 3 MPa is of best operational measure.

Table 2.4: Relation of $CO2$ inlet pressure with the yield and current efficiency in an undivided cell at room temperature, c: current density [23]

Sr. no.	CO_2 pressure (MPa)	Isolated Yield (%)	η (%)[c]
1	1	65	32.5
2	2	83	41.5
3	3	84	42
4	4	83	41.5
5	5	82	41

2.5. State of the Art Research

The research by Neumann et al. serves as a patented production method for 3-hexenedioic acid [36]. The patent describes a method for the electro-dicarboxylation of at least one diene with carbon dioxide

in the presence of hydrogen, leading to the formation of at least one unsaturated dicarboxylic acid. The reaction takes place in an electrolyser that includes a working electrode for the cathodic activation of CO_2 and a counter-electrode for the oxidation of hydrogen. The hydrogen to CO_2 volumetric ratio is maintained between 1:1 and 1:3, with the reactor's total pressure ranging between 2 and 4 MPa. The method is performed within the range of the current density of 5 to 15 mA/cm², preferably between 10 and 12.5 mA/cm², to optimise the reaction conditions.

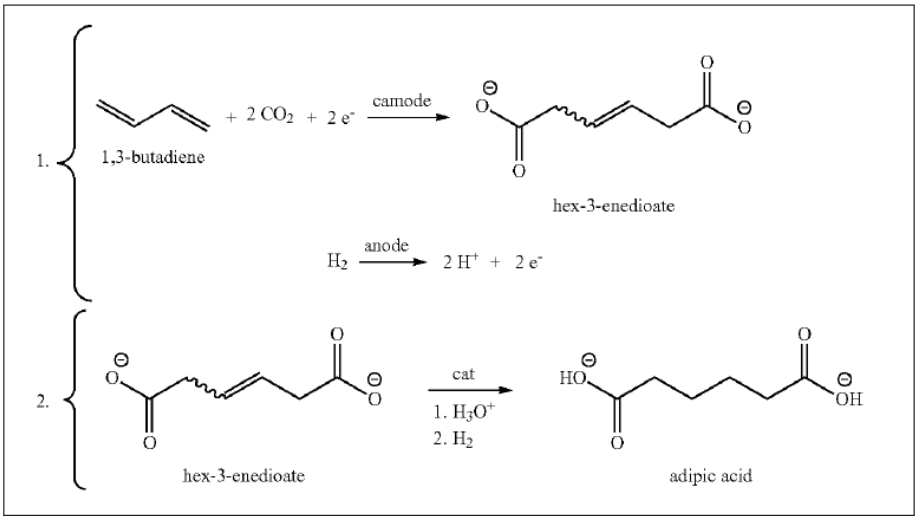

Figure 2.6: Scheme for electrodicarboxylation of 1,3-butadiene with CO_2 comprising Hydrogen at anode [36]

The scheme in the patent uses hydrogen as a reducing agent. The catalysts for reaction feasibility are platinum, activated carbon, silica, titanium dioxide or the Wilkinson catalyst. This avoids to use of sacrificial anodes and, subsequently, curbs the expenditure to replace the spent aluminium and its salts from the reactor [36]. The cathode used is graphite or transition metals like Nickel or Platinum with DMF as the electrolyte. However, the byproduct formation of monocarboxylic acids is increased with this process. The patent states the increase in the faradaic efficiency of products by the use of mediators like RhCl, PdCl2, PdCl3, and Fe.

The recorded faradaic efficiencies lie in an appreciable range of 20-25 % for all carboxylated products and between the range of 15-20 % for unbranched dicarboxylic acid products. Additionally, the patent claims at formation of predominant trans isomers of 2-HDA, 3-HDA and 3-Methyl-pentenedioic acid. It states that at adequate pressures between 3-4 MPa, the product distribution for 3-PA can be suppressed. The patented process is developed with a motive to operate continuous processes for better production rates.

In conclusion, for the literature review, various factors and parameters that influence the product distribution or selectivity, yield and faradaic efficiency are broadly studied and specified for different case scenarios. Further, in the experimentation stage, the primary aim will be to employ a strategy to mimic results from certain papers for producing 3-HDA and attempt to improve the faradaic efficiency. This will be followed by subsequent optimisation attempts motivated by the backing of literature, like the use of electrocatalysts and electrode material, along with system conditions that improve product selectivity and efficiency.

3

Methodology

The objective of presenting a methodology is to provide knowledge of the experimental procedure employed and analytical techniques used in the thesis for studying the synthesis of 3HDA. The literature review from the Chapter 2, renders the foundation for the design of experiments, primarily to study the synthesis of 3HDA in a controlled system environment, and subsequently optimising the electrolyser parameters.

This chapter outlines the selection of electrode materials, reaction conditions, reactant concentration, supporting electrolyte concentration, and cell design. Additionally, highlighting how the variables affect the faradaic efficiency and selectivity of the product. Faradaic efficiency monitoring remains a key factor for the majority of the thesis analysis as it allows for understanding the number of electrons contributing to the formation of the desired product, 3HDA. It is also a KPI as the project is based on providing an overview of how high-value chain products can be manufactured using renewable electricity.

Furthermore, the chapter provides a brief overview of how analytical techniques like Cyclic Voltammetry (CV), Chronoamperometry (CA), and Chronopotentiometry (CP) enable analysis of critical factors like reduction potentials, onset potential, overpotential, and current densities during electrolysis. Analytical techniques like in-line Gas Chromatography (GC), High Performance Liquid Chromatography (HPLC), and Liquid Gas Chromatography (LGC) are used to quantify to product formed and serve data used to calculate the selectivity, yield, isolated yield and faradaic efficiency of the product and by-products. Additionally, experimental analysis using the Crystal16 machine is done as a basis for understanding the dissolved product limits. These methods are essential for understanding the electrochemical behaviour of the system and ensuring the desired products are obtained with high efficiency.

The chapter begins with understanding how the electrochemical set-up is designed to break down the step-wise formation of the product, which is mentioned in the mechanism section 2.2 of the literature review.

3.1. Electrochemical Set-up

The process for the synthesis of 3HDA is predominantly evaluated by the electrochemical activation of CO_2 at the cathode. For CO_2RR, two-electrode systems (working and counter electrode) and three-electrode systems (working, reference and counter) are often debated.

Two-electrode set-ups are simple but can cause complexities in results and thus analyses, as they record the complete voltage drop by the current across the entire cell. It can be a suitable option when the counter electrode potential is expected not to drift during the experiment, and often when low current densities are expected. Whereas in three-electrode set-ups, the voltage drop is not between

the counter and working electrode but instead between the working and reference electrode. The reference electrode is the experimental reference point and thus holds a constant voltage against the working electrode, ideally absolute, and current does not flow through it [17]. The isolated voltage allows the study to be of greater accuracy, thus giving an experimental advantage over the two-electrode system.

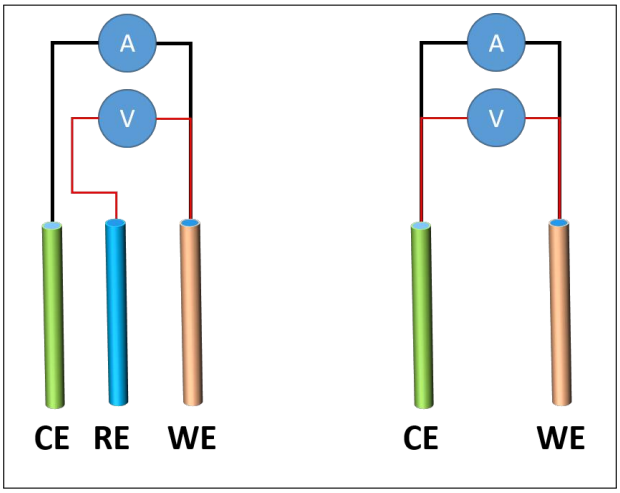

Figure 3.1: Two-electrode and three-electrode set-up, where CE: counter electrode, WE: working electrode, and RE: reference electrode [21]

Figure 3.1 shows how the voltage is applied across the reference and working electrode, but the current flows through the counter and working electrode. When the voltage drop is accurate, phenomena like the activation energy and catalytic properties of the working electrode can be examined at a deeper level.

As described in the literature review, nickel as a working electrode is best suited for the electroreduction of CO_2 for dicarboxylation of conjugated dienes. Additionally, research provides basic results where the nickel cathode enables reaching higher faradaic efficiency and better yield percentages. Thus making it the best choice for the cathode in producing 3HDA. One of the most stable, reliable, and available reference electrodes is Ag/AgCl, which is also leak-proof. Among Mg and Al in contention for sacrificial anodes, as they have better C6 selectivity, Aluminium is chosen to be employed in the experiments, as it is cheaper and widely available.

From Table 2.3 of the literature review, the highest efficiency is gained when organic electrolyte solvents like acetonitrile (CH_3CN) or N,N-dimethylforamide (DMF) are used. Moreover, it supports the selectivity of the C6 product for which the process is designed. Acetonitrile has a large stability window and lower degradation at higher negative potentials, thus disallowing more unwanted side product formation. It is also less viscous and has high CO_2 solubility [42]. The dielectric constant for acetonitrile is also high, around 35.09 at room temperature, making it a top choice of electrolyte solvent to be used [30]. Acetonitrile is also compatible with most supporting electrolytes like tetraalkylammonium salts and provides better ionic conductivity [26]. Being aprotic and possessing lower water content [9] makes it the best choice for application and is thus chosen for preliminary experimentation.

Among the tetraalkylammonium salts used as supporting electrolytes for the efficient electroreduction, tetraethylammonium chloride (TEACl) is chosen for application in the cell with a concentration of 200 mM. The concentration plays a major role in the setup as it affects the resistance, conductivity, mobility of ions, etc. The desired concentration is chosen by experimental procedure, and the concentration is increased from 100 mM onward to check for the C6 product formation. TEACl, being a relatively smaller cation, provides higher ionic mobility and minimises ion pairing with the intermediate radical

anions compared to that of tetrabutylammonium (TBA+) or tetrahexylammonium (THA+) supporting electrolytes [10]. Having a lower ion pairing affinity allows the intermediates to successfully participate in the purposeful reaction.

Employing all the above electrode, electrocatalyst and electrolyte conditions, it makes a strong case to use an undivided cell for the electroreduction of CO_2 with 1,3-butadiene. Thus, an unidivided electrochemical cell with a three-electrode introduction system is chosen for its non-fallible positive impacts on the selectivity of C6 product and efficiency. It is a 50 ml capacity high borosilicate glass sealed electrochemical cell and has a 5-opening lid, 3 for the electrodes and the rest for continuous introduction of CO_2, the excessive reagent, and for the in-line GC connection [11] as observed in Figure 3.5. Pressure variation in this cell is not possible as it is not designed to withstand higher pressure; thus, the CO_2 inlet is a low pressure stream. Temperature can be varied by external means, like surrounding the cell with a water bath and allowing thermal equilibrium with continuous stirring and time extension.

Figure 3.2: 3 electrode system electrochemical cell withCO_2 inlet and in-line GC connection

After the electrochemical set-up is finalised, the process conditions and parameters need to be understood and studied. Techniques for realising the process parameters and mechanism, subsequently for monitoring the reaction kinetics, are stated in the next section, and for evaluation of the product based on faradaic efficiency and yield are explained.

3.2. Electrochemical Process Techniques and Parameters

To understand the reduction potential, current density because of the cathode, anode and electrolyte used, and to synthesise the desired product, the three most basic techniques in electrochemical systems are cyclic voltammetry (CV), chronoamperometry (CA) and chronopotentiometry (CP).

3.2.1. Cyclic Voltammetry

Cyclic voltammetry is widely used for measuring the resultant current, as the potential of the working electrode sweeps back and forth between two set values [13]. This produces a characteristic duck-shaped plot known as a cyclic voltammogram [27]. For experimentation of the thesis, cyclic voltammograms are recorded between -1 V to -3 V as CO_2 reduces between -2.2 V to -2.5 V against Ag/AgCl, as observed from Figure 2.3 as the focus is to check the reduction potential and current for CO_2 and 1,3-butadiene. The CV is performed for four readings, viz., blank electrolyte solution with argon deaeration, electrolyte solution with CO_2 saturation, electrolyte solution with 1,3-butadiene addition and argon deaeration, and electrolyte solution with 1,3-butadiene addition and CO_2 saturation. The cyclic voltammogram curve for the electrolyte solution with 1,3-butadiene addition and CO_2 saturation is ideally monitored for the onset potential. Onset potential is the potential at which the feasibility for activation of reactants begins. Secondly, the electrolyte solution with 1,3-butadiene addition and CO_2 saturation curve is monitored to be closer to the electrolyte solution with CO_2 saturation or the electrolyte solution with 1,3-butadiene addition and argon deaeration to comment on the plausible reaction mechanism pathway of the radical anion formation and the subsequent nucleophilic attack [7]. Lastly, the potential for the electrolyte solution with argon deaeration is checked, as that potential range is where the electrolyte solution is expected to degenerate, leading to possible unwanted side product formation. Once the onset potential is determined, chronoamperometry is performed for a range of potentials about the onset potential for determining the reduction potential at which the faradaic efficiency is the best.

3.2.2. Chronoamperometry

Chronoamperometry is a technique where a step potential is applied within the range decided about the onset potential, to study the resultant current as a function of time. The electrode area is a factor in the kinetics of the reaction; hence, the usual representation is for current density as a function of time. By analysing the current density, the rate of the reaction can be understood [19]. The reaction rate determines the amount of 1,3-butadiene converted during the time of reaction. Two phenomena are observed in the current density curve: decay and surge in current. Decay of current means a decrease in current over time of reaction, indicating sluggish reaction kinetics or rate limitation or product accumulation. Surge in current, as the name suggests, is an increase in current density over the time duration of reaction, indicating a faster rate of reaction and efficient electron transfer at the electrode-electrolyte interface. The faster or slower reaction kinetics can be used to comment on the product selectivity at a particular rate of reaction. The charge consumed by the reactants throughout reaction time allows further determination of the faradaic efficiency towards the synthesised products, and specifically towards 3HDA.

3.2.3. Chronopotentiometry

Chronopotentiometry is a technique used to monitor the potential as a function of time, keeping the current constant [28]. It is used to study the reaction kinetics and to understand the stability of the working electrode and the point of passivation, which is critical for planning the operational parameters. The reactants migrate to the working electrode to balance the applied current until it gets completely used up, allowing other species to be reduced if at all present in the cell and have affinity to be reduced in the same environment. This also shifts the potential, indicating the reduction of other species. The potential curve also allows for the study of the overpotential at a particular current density that was observed in the chronoamperometry test.

Both chronoamperometry and chronopotentiometry are employed to check for certain criteria mentioned in the above paragraphs. During the tests, the reactants are converted to products, alongside the voltage or current being monitored. Chronoamperometry is mainly used for understanding the current taken and the electrons contributing to the synthesis of the favoured C6 product. There are products in solid, liquid and gaseous form. 3HDA (C6) and 3PA (C5) are primarily detected in solid product as 3HDA is crystalline in nature at room temperature. The in-line GC monitors the gaseous products, and the liquid and solid products are separated by centrifugation after the CA or CP test. The solid products are analysed by techniques like HPLC, and the products in the supernatant are analysed

using Liquid GC, which is described in the following section.

3.3. Analysis Techniques

Various gaseous, liquid, and solid products of the reaction are examined using in-line GC, HPLC and Liquid GC techniques, respectively. These analyses serve as a basis to calculate the selectivity, yield, isolated yield and faradaic efficiency of the products formed during the reaction.

3.3.1. High Performance Liquid Chromatography

For product analysis, the primary technique used is high performance liquid chromatography (HPLC) as the 3HDA product found in the solid sample is dissolved in an eluent for analysis. In HPLC, peak formation is governed by the interplay of chromatographic parameters such as column chemistry, mobile phase composition, and flow rate. A well-resolved peak with baseline separation indicates efficient interaction between the analyte and the stationary phase, minimising co-elution of impurities. Elution order depends on analyte polarity, with hydrophobic compounds typically retained longer on reversed-phase columns under gradient conditions [39]. For peak identification, retention time matching with reference standards is combined with UV spectral analysis using a diode array detector (DAD) to confirm purity [25]. However, ambiguous peaks would require other advanced techniques like LC-MS (Liquid Chromatography-Mass Spectroscopy) to resolve co-eluting species and verify molecular identity via mass-to-charge ratios [4].

In the HPLC system, the peaks for the desired products are observed on the 1-hour injection timeline. Elution point for the 3HDA peak is between 28.2 to 28.4 minutes, the 3PA peak is between 51.4 to 51.8 minutes, the oxalic acid peak is between 11.8 to 12.1 minutes, and the formate peak is between 27.4 to 27.8 minutes. The retention time of elution points varies moderately based on the pH of the sample [39]. For a better approximation of the peak, every vial is injected twice in the HPLC, and the average of the two areas is considered for analysis. The calibration curves for 3HDA, 3PA, oxalic acid and formate are attached in the Appendix A.2. The quantification of the peaks into the amount of product formed is done using the calibration curves generated from known concentrations.

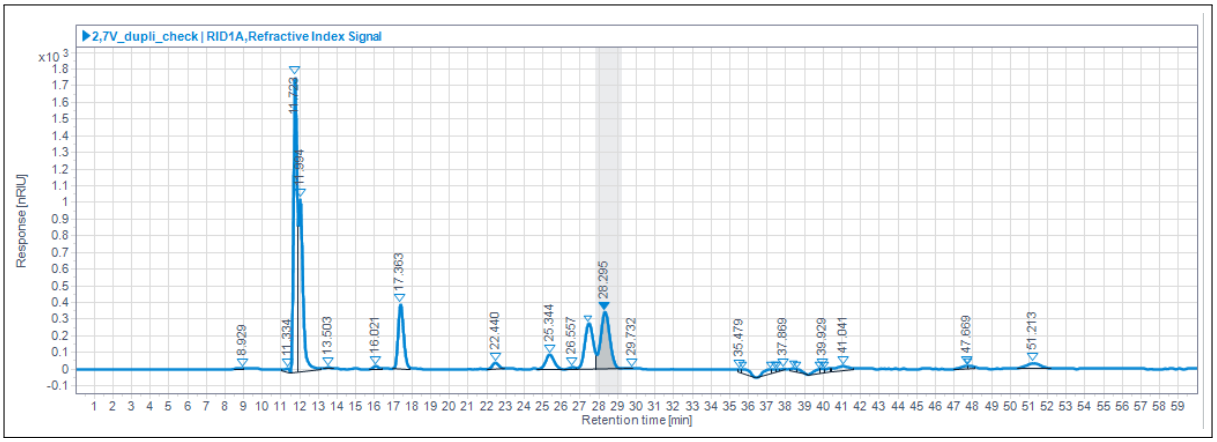

Figure 3.3: HPLC Chromatogram - (a) 11.994 minute is oxalic acid peak, (b) 27.4 minute is formate peak, (c) 28.295 minutes is 3HDA peak, (d) 51.213 is 3PA peak

3.3.2. Gas Chromatography

For analysing the gaseous products such as CO, CO_2, H_2 and other gases produced during the experiments, in-line gas chromatography using the Global Analyser Solutions CompactGC 4.0 provides a robust method for real-time monitoring of the produced gases escaping the electrochemical cell. The CompactGC 4.0 is engineered for high-throughput gas analysis, delivering results with a fast injection system, narrow-bore columns, and highly sensitive detectors such as the thermal conductivity detector

(TCD) and flame ionisation detector (FID). The instrument uses three independent analysis channels (FID, TCD2 and TCD3), allowing simultaneous detection and quantification of multiple gases, including permanent gases and light hydrocarbons [14]. During operation, the gas sample is introduced directly from the process stream into the CompactGC 4.0, where it is rapidly injected onto the chromatographic column in an injection time of 2 minutes each. The separation of gases occurs based on their interaction with the stationary phase and their respective volatilities, resulting in distinct elution times for each gas. The elution point for H_2 is at 0.487 minutes, 0.597 minutes is for CO and 0.754 minutes is for CO_2.

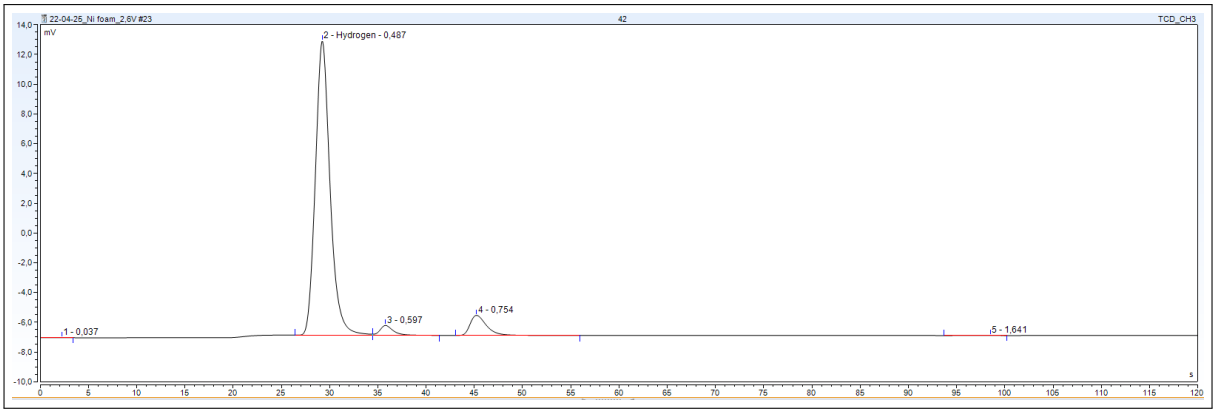

Figure 3.4: GC Chromatogram - (a) 0.487 minutes is H_2 peak, (b) 0.597 minutes is CO peak and (c) 0.754 is unreacted CO_2 peak

Peaks corresponding to CO, CO_2, H_2 and other detected gases are quantified using the integrated data system of Chromeleon, which provides real-time chromatograms [37]. The detector produces a voltage response as each gas elutes from the column, forming a peak whose area is directly proportional to the amount of that gas present in the sample [16]. The CO and H_2 peaks are observed in the TCD3 channel with an area plot of 'mV * time', where time is the retention time of the gas at elution point (on the x-axis). The high sensitivity and repeatability of the CompactGC 4.0 enables the detection from sub-ppm to percentage levels, supporting both trace analysis and bulk quantification [14]. The flow rate meter between the process system and the in-line GC determines the volumetric flow of gases, based on which the faradaic efficiency towards the gases can be quantified. This helps especially to estimate the amount of CO and H_2 formed and how other products are impacted because of the HER.

3.3.3. Liquid Gas Chromatography

For analysing the unreacted 1,3-butadiene and dissolved products in the supernatant using the Agilent Technologies 7890A Liquid GC, gas chromatography provides a sensitive and selective approach for both qualitative and quantitative assessment. Typically, a sample of the supernatant is introduced into the GC via a suitable injection method like a high-pressure liquid injector (HPLI) or a split/splitless inlet, ensuring efficient vaporisation and transfer of volatile analytes such as 1,3-butadiene and its hydrocarbon impurities [2]. Liquid GC can also be employed to detect the dissolved 3PA (C5 product) in the supernatant.

The column is maintained at an optimised temperature program to resolve 1,3-butadiene from other volatile and semi-volatile products. Detection is typically performed with a flame ionisation detector (FID), providing excellent sensitivity for hydrocarbons. For supernatants containing high concentrations of 1,3-butadiene, method adaptations such as post-column backflushing can be used to reduce analysis time and prevent late-eluting impurities from contaminating the column or detector, thereby improving retention time reproducibility and overall analytical cycle time [2]. The use of particle trap technology in the GS-Alumina PT column further enhances method stability and minimises maintenance by preventing particle-induced blockages [3]. The 1-hour cycles are set for every injection per vial. Peaks are identified by comparing retention times to those of reference elution points, while quan-

tification is based on calibration curves generated from known concentrations. The elution time for 1,3-butadiene is between 11.1 to 11.3 minutes, and that of 3PA is between 14.1 to 14.4 minutes. The calibration curves for the compounds are attached in Appendix A.3.

3.3.4. Crystal16

The Crystal16 is a state-of-the-art parallel crystallisation equipment designed to rapidly and accurately determine solubility curves and crystallisation conditions for a wide range of compounds, including pharmaceutical and chemical products. With Crystal16, users can simultaneously screen multiple concentrations and solvent systems, significantly accelerating the process of solubility determination. This system features 16 independent reactors, each accommodating a standard 2 mL vial scale, allowing for medium-throughput studies with minimal material, often less than 100 mg per experiment [34]. Crystal16 is a polythermal method of analysis used to determine the temperature at which a salt or compound is completely soluble in a solvent. In the thesis, it has been to study the solubility of solutions of certain concentrations of 3DHA in the supernatant, as mentioned earlier in the subsection 3.3.1. Crystal16's core innovation lies in the integration of automated temperature control and transmissivity measurement, which enables precise detection of clear and cloud points as a function of temperature. These measurements are crucial for constructing solubility curves of a compound in the solvent [35]. For each concentration, Crystal16 gives a temperature range with minimal error, where 3HDA is completely soluble in the supernatant. Most of the chronoamperometry experiments are conducted at room temperature, and thus, an estimate of the concentration of 3HDA, being the maximum limit dissolved in the supernatant at a particular temperature, can be used for further analyses.

3.4. Experimental Methodology for Synthesis

The first experiment plan is inspired from the theory in Chapter 2 and the subject matter mentioned in section 3.2 and section 3.3. A good know-how of electrochemical experiments is developed to strategically design the synthesis of products using the techniques mentioned in prior sections. For undivided cell electrolysis, Li et al. have maintained a 70 mM concentration of 1,3-butadiene in the electrolyte, reporting an isolated yield of 84% and a faradaic efficiency of 42% [23]. For better analysis of the conversion and the product selectivity within the solid product in a testing window of a couple of hours of chronoamperometry, the 1,3-butadiene concentration in the electrolyte is kept at 150 mM. This also allows greater availability of 1,3-butadiene in cases where the reaction mechanism follows butadiene radical anion formation at the cathode and followed by its attack on CO_2.

In the prior lab work, the supporting electrolyte concentration was controlled between 100 mM to 200 mM for tetraalkylammonium salts. Enough electrolyte conductivity leads to an efficient reaction at 200mM concentration, and thus the electrolyte concentration is kept uniform throughout the experimental plan. Thus, keeping the other parameters the same as stated in the section 3.1, the first set of experiments is finalised. The materials and chemicals, fixed parameters and procedure for the experiments are mentioned in the following subsections.

3.4.1. Experiment Materials and Reactants

To prepare the electrolyte solution, TEACl is dried overnight in an oven before every experiment due to its hygroscopic nature. The 200 mM electrolyte solution is freshly prepared with TEACl and acetonitrile before every experiment. The electrolyte solution is saturated with Argon (Linde, 5.0 purity), or CO_2 (Linde, 5.0 purity), depending on the test to be performed. Prior to all the experiments, the electroylsis cell and required glassware is thoroughly cleaned with water and acetone (Sigma Aldrich EMPLURA, >=99%) and dried in an oven for atleast 30 minutes before use.

For the optimisation experiment set, the water used is ultrapure (IQ7000 MilliQ grade, >=18.2 $M\Omega.cm$). Additonally, for certain experiments, dry acetonitrile (Thermo Scientific, 99.9%, extra dry over molecular sieve, Acroseal) is used. For experiments with different supporting electrolytes, $TBABF_4$ (Sigma Aldrich, 99%) and $TBAPF_6$ (Sigma Aldrich, 98%) are used with acetonitrile (Sigma Aldrich, >=99.9%) as the electrolyte solution. For a set of experiments copper wire of 2 mm diameter (MaTeck GmbH, 99.99%) is used as a working electrode instead of nickel. The copper electrode needs to be activated before

use, which is done using the method mentioned by Kumar et al. [20]. Copper wire is initially polished using sandpapers of grades P320, P800, P1200, and P2000 for the removal of the oxidised layer. The copper wire is further mechanically polished using 1μm polycrystalline diamond suspensions (MetaDi Supreme) and 3 μm monocrystalline diamond suspensions (Struers). For removal of trace impurities, it is ultrasonicated in isopropanol (Sigma Aldrich EMPLURA, >=99.5%) and later dried with argon gas (Linde, 5.0 purity) flushing. The polished and cleaned copper electrode is later electropolished at an oxidation potential of 2.1 V against a carbon rod as counter and reference electrode in phosphoric acid (Sigma Aldrich, BioUltra >=85%). Chronoamperometry is performed for 3 minutes and then removed and cleaned with MilliQ water, and dried thoroughly with Argon for a minute to remove the moisture from the electrode surface. After the activation and electropolishing, the copper electrode can be used exactly like the nickel electrode in the experimental setup.

3.4.2. Experimental Measurement

The electrochemical experiments were conducted using a sealed single compartment electrochemical cell configuration with carefully selected materials and chemicals to synthesise the dicarboxylation of 1,3-butadiene with CO_2. The working electrode used was a nickel wire of 0.5 mm diameter (MaTeck, 99+%), chosen for its superior catalytic performance, while an aluminium wire coil of 2 mm diameter (MaTeck, 99.95%) served as the sacrificial counter electrode. A commercial leak-free Ag/AgCl (Alvatek) reference electrode was employed to enable accurate potential control. The electrolyte solution comprised 200 mM tetraethylammonium chloride (TEACl)(Sigma Aldrich, >=98%) dissolved in 38 ml of acetonitrile (MeCN) (Sigma Aldrich, >=99.9%), and saturated with CO_2 (Linde, 5.0 purity) for 30 minutes. The reactant solution contained 150 mM 1,3-butadiene (Sigma Aldrich, 20 wt.% solution in toulene) and was continuously bubbled with CO_2 (Linde, 5.0 purity) at a rate of 8 ml/min to ensure constant reactant availability during the reaction.

Cyclic Voltammetry is performed for a set of experiments as mentioned in section 3.2.1 and once the onset potential is identified, chronoamperometry tests are performed for a step difference voltage around the onset potential as mentioned in section 3.2.2. For studying the electron to product relation, chronopotentiometry is performed in a certain case for as mentioned in section 3.2.3. After conducting the CA or CP tests, the synthesised solid products are formed which can be identified from the turbid nature of the reaction solution in Figure 3.1. Since 3HDA is naturally crystalline in nature at room temperature, it is ideally synthesised as a solid product.

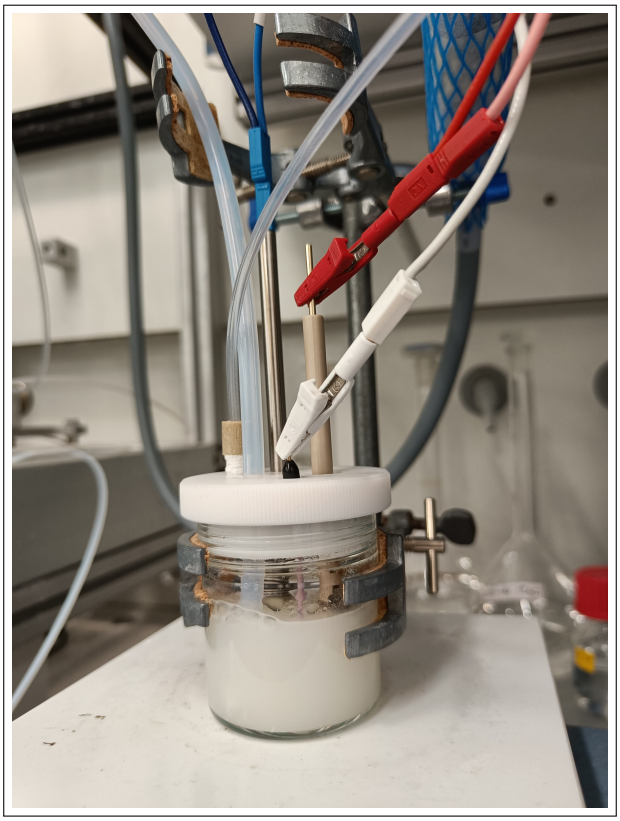

Figure 3.5: Electrochemical cell after 2 hours of chronoamperometry/chronopotentiometry

The process liquid is centrifuged to separate the solid product from the liquid product in Universal 320R of Hettich Zentrifuger, which is then washed thoroughly with acetonitrile and dried overnight in a fume hood. The sample is then weighed, as it is important for calculating the faradaic efficiency and yield which can be understood from Appendix A.1.

1 to 2 milligram of dried sample is dissolved in 5 mM H_2SO_4, which is a mobile phase eluent and 0.5 M NaOH for enhanced dissolution. The sample is further tested for 3HDA, 3PA, oxalic acid, and formate in HPLC Agilent 1260, Infinity II. The SOP for HPLC quantification is followed and the peak area is observed as mentioned in section 3.3.1. The peak are is used for calculating the product concentration using the HPLC curves from Appendix A.2. The concentration of solid product is considered for calculating the faradaic efficiency, product selectivity or distribution, yield and isolated yield using the step-wise method mentioned in Appendix A.1.

After gaining insights into the procedure to perform the experiments, the report progresses to the results of various set of experiments explained in the section 3.4, and the analyses. The performed experiments aim to answer the research questions, which are supported by the results presented in the subsequent chapter.

4

Results and Discussion

This chapter focuses on understanding the results of the conducted experiments to evaluate the product distribution of the solid product, followed by analysing the faradaic efficiency, especially for 3HDA and studying the effects of reaction rate kinetics and the plausible mechanism of the reaction on the synthesised product. After subsequent analysis of the faradaic efficiency and other factors for the primary set of experiments mentioned in section 3.4.2, optimisation strategies are employed with an aim to improve the faradaic efficiency of the C6 product.

4.1. Nickel Wire Cathode

4.1.1. Chronoamperometry

Cyclic voltammetry was performed to identify the electrochemical behaviour of the system under various reactant environments and to estimate the appropriate potential window for subsequent chronoamperometry experiments. The blue and green CV curves show cathodic current gained about the same potential, around -2.4 V, highlighting that the reaction may proceed via 1,3-butadiene activation at the cathode and butadiene radical anion attacking CO_2. The green CV trace further reveals a sharp increase in cathodic current beyond -2.4 V, defining the onset potential for electroreduction and the range where the significant reaction occurs. Thus, potentials from -2.4 V to -2.8 V were selected for the chronoamperometry test to study both, onset and high-driving-force regimes. The cyclic voltammogram in Figure 4.1a confirms that the electroreduction of CO_2 and 1,3-butadiene is feasible within the selected range, and the magnitude of current suggests increasing activity with more negative potentials.

Chronoamperometry was employed to investigate the electrochemical reduction behaviour of CO_2 and 1,3-butadiene at a nickel wire working electrode using an aluminium coil as the counter electrode. The experiments were conducted at five step potentials ranging from -2.4 V to -2.8 V vs. Ag/AgCl to evaluate their influence on current density, product distribution, and faradaic efficiency. Figure 4.1b presents the CA curves, revealing distinct trends in current density over a 120-minute experiment. At higher reduction potentials of -2.7 V and -2.8 V, a greater initial current density was observed, which subsequently flattened and stabilised, indicating an early surge in electrochemical activity followed by product accumulation at the cathode or electrode surface passivation. In contrast, for lower reduction potentials between -2.4 V and -2.6 V, the current density increased in magnitude as the time progressed, indicating slower initial kinetics but efficient mass transfer throughout the duration of the reaction. At early timestamps between 0 and 20 minutes, approximately, the sharp current drop partly reflects capacitive charging because of the double layer effect, especially observed in organic electrolytes. The excessive noise in the CA curves is because of the CO_2 inlet bubbles, and the bubbles that are caused by the gaseous products formed at the cathode. Another reason for the noise in the current density is the

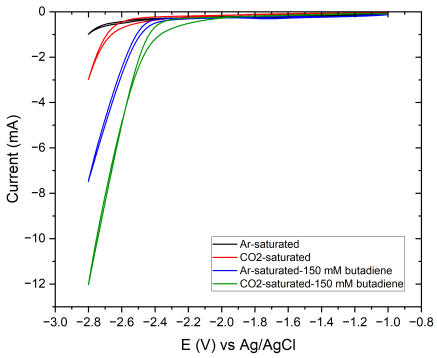

(a) Cyclic Voltammetry for nickel wire and aluminium coil in acetonitrile and tetraethylammonium chloride electrolyte solution (200 mM) with (a) (black) blank electrolyte solution, (b) (red) CO_2 saturated electrolyte solution, (c) (blue) Argon deaerated and 1,3-butadiene added electrolyte solution (150mM), (d) (green) CO_2 saturated and 1,3-butadiene added electrolyte solution (150mM)

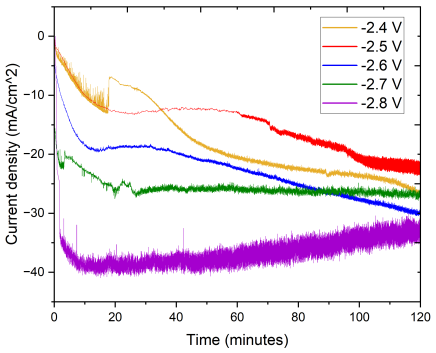

(b) Chronoamperometry experiments at potentials of (a) (yellow) -2.4 V vs Ag/AgCl, (b) (red) -2.5 V vs Ag/AgCl,(c) (blue) -2.6 V vs Ag/AgCl,(d) (green) -2.7 V vs Ag/AgCl, (e) (magenta) -2.8 V vs Ag/AgCl conducted for 120 minutes, working electrode area is 0.32 cm^2, 200 mM electrolyte solution of acetonitrile and tetraethylamonium chloride with CO_2 and 1,3-butadiene addition (150 mM)

Figure 4.1: (a) CV and (b) CA plots for acetonitrile and tetraethylammonium chloride with nickel wire and aluminium coil as working and counter electrode, respectively

setting for reading the current change per unit of time in the EC-Lab software.

Since an electrochemical surface area of 0.32 cm^2 of the cathode was used, the observed current densities are relatively high for a nickel wire, suggesting efficient charge transfer per unit area. The surface area for nickel wire is approximated by an assumption that about 2 cm of nickel wire cathode is dipped in the electrolyte for the experiments. This supports nickel's suitability for improved CO_2RR kinetics and thus showcases efficient electrocatalytic properties.

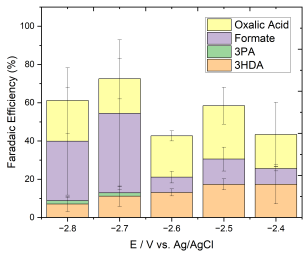

(a) Faradaic efficiency in '%' for products of the reaction at different potentials of CA experiments

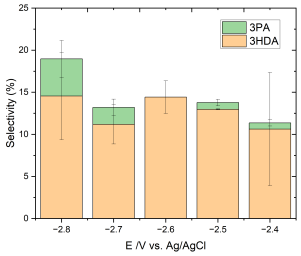

(b) Selectivity in '%' for C5 and C6 products of the reaction at different potentials of CA experiments

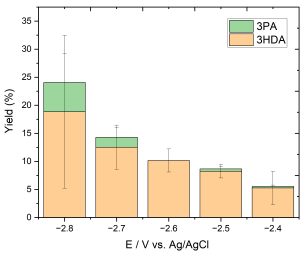

(c) Yield in '%' for C5 and C6 products of the reaction at different potentials of CA experiments

Figure 4.2: Faradaic efficiency, selectivity, and yield for products of the reaction at different potentials of the CA experiments for the nickel wire working electrode

The faradaic efficiency of each solid product was calculated using the HPLC peak area, and that can be observed in Figure 4.2a. The maximum combined faradaic efficiency is observed at -2.7 V. A clear trend emerged for the faradaic efficiency of 3HDA, which reduces from -2.4 V to -2.8 V. At -2.8 V, with faradaic efficiencies around the same ballpark for reduction potentials between -2.4 V and -2.6 V. Although current densities were high, faradaic efficiency dropped due to the formation of side products such as formate and oxalic acid, likely promoted by increased proton availability or CO_2 dimerisation, respectively. The rest of the faradaic efficiency is going to the gaseous products formed, like H_2 and CO.

This highlights the importance of studying the selectivity of products or the product distribution, especially for the C5 and C6 products. In Figure 4.2b, the selectivity of 3HDA lies in the range of 10 to 15 % across reduction potentials, and is peaked at -2.6 V. For 3PA, the selectivity increases from -2.4 V to -2.8 V, with an abnormality at -2.6 V. The trend suggests that the monocarboxylated product of 3PA is more dominant at higher potentials. Since there is no 3PA product formation and only 3HDA is formed at -2.6V, it can be regarded as a potential at which conjugated diene is undergoing complete decarboxylation, and serving 100% of 3HDA among the carboxylated products.

The yield for C5 and C6 products follows a similar trend seen in Figure 4.2c, where the yield increases almost arithmetically from -2.4 V to -2.8V. The yield is calculated only based on the product formed among the mix of solid products.

4.1.2. Chronopotentiometry

Chronopotentiometry was performed to understand the voltage response of the nickel wire electrode under constant current conditions and to evaluate how varying applied current influences the stability of the working electrode potential, and subsequently, the distribution and efficiency of products. The experiments were conducted at four different currents of 10 mA, 15 mA, 20 mA, and 25 mA (current densities: 31.25 $mA \cdot cm^{-2}$, 46.875 $mA \cdot cm^{-2}$, 62.5 $mA \cdot cm^{-2}$, and 78.125 $mA \cdot cm^{-2}$, respectively) for 120 minutes of reaction time. The working electrode's electrochemical surface area was fixed at 0.32 cm².

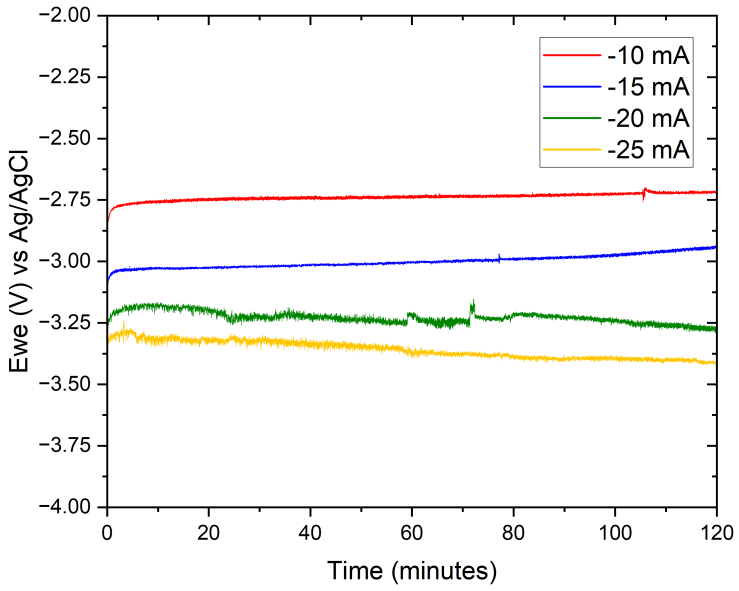

Figure 4.3: Chronopotentiometry tests at current of (a) (red) 10 mA, (b) (blue) 15 mA,(c) (green) 20 mA, (d) (yellow) 25 mA, conducted for 120 minutes (on the x-axis) and the reduction potential (on the y-axis), working electrode area is 0.32 cm^2, 200 mM electrolyte solution of acetonitrile and tetraethylamonium chloride with CO_2 and 1,3-butadiene addition (150 mM)

At 10 mA current, the potential is quite stable around -2.75 V, indicating that the electrode is not passivated and there is a balanced rate of electron transfer and reactant consumption. At 15 mA, the potential marginally drifts between −3.05 to −2.95 V vs Ag/AgCl, which suggests improved electrode kinetics and the electrode providing better activation conditions for CO_2 and 1,3-butadiene as the reaction progresses. At higher currents of 20 mA and 25 mA, an increase in reduction potential by 0.2V, indicating overpotential, suggests electrode instability and mass transport limitation, which can lead to unnecessary side reactions. The vast difference in potential from -10 mA to -25 mA is because accord-

ing the Butler-Volmer equation and Tafel Slope behaviour, when the current taken is beyond the ohmic region, the system leads to overpotential, which is nonlinear in nature.

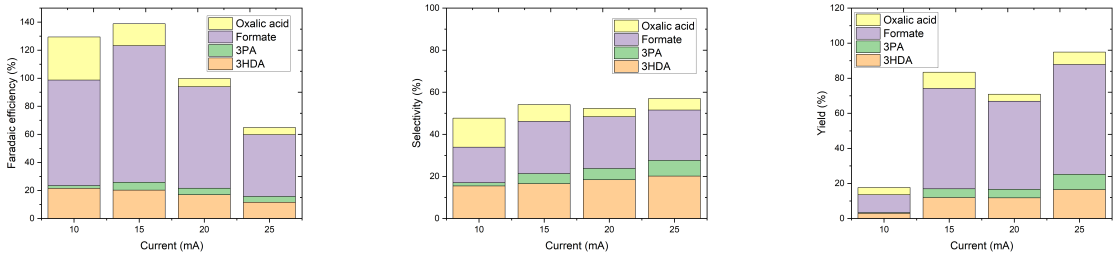

(a) Faradaic efficiency in '%' for products of the reaction at different currents of CP experiments

(b) Selectivity in '%' for products of the reaction at different currents of CP experiments

(c) Yield in '%' for products of the reaction at different currents of chronopotentiometry experiments

Figure 4.4: Faradaic efficiency, selectivity, and yield for products of the reaction at different currents of the chronopotentiometry experiments for the nickel wire working electrode

It is observed that at higher currents, the system is dominated by side reactions, and the faradaic efficiency for 3HDA in Figure 4.4a, shows a decreasing trend as the current is increased. Also, the combined faradic efficiency of solid products decreases between 15 mA and 25 mA, indicating more gaseous product formation, like the HER being prominent. Additionally, the faradaic efficiencies rising above 100% are because of the overlapping HPLC peaks of oxalic acid and CO_2 reactant being available in excess in the electrochemical cell.

The selectivity distribution remains relatively stable across the tested currents with a slight increase in selectivity of 3HDA and a major increase in 3PA product selectivity as the current is increased, observed in Figure 4.4b. Thus indicating higher monocarboxylation and incomplete reactions at higher current densities. The highest combined yield is observed for the highest current of 25 mA, but mainly the yield consists of oxalic acid and formate, rendering it undesirable for the current to be that high. The trend for 3HDA yield increases drastically from 10 mA to 15 mA, and a similar yield at currents between 15 and 22 mA, observed in Figure 4.4c.

Considering the faradaic efficiency and product selectivity, 10 mA is a better current for 3HDA production. The maximum selectivity of 3HDA among the carboxylated products is at 10 mA, which is 31.25 $mA \cdot cm^{-2}$ current density. Circling back, the current density achieved for the chronoamperometry test at a potential of -2.6 V is about 31 $mA \cdot cm^{-2}$ as well. Thus, underpinning that the conditions where the electrode remains stable for the chronoamperometry test for the entire duration of the reaction, a constant current can be assumed. This favours the selection of -2.6 V as the prime reduction potential for chronoamperometry with a nickel wire cathode. Additionally, the reduction potential in the chronopotentiometry test for 10 mA current is -2.75 V, that is 0.15 V higher than -2.6 V. This indicates that overpotential allows room for monocarboxylation, as 100% selectivity of C6 product among the carboxylated products was achieved at -2.6 V.

After subsequent analysis of the faradaic efficiency and other factors for the primary set of experiments with nickel wire electrode, optimisation strategies are employed with an aim to improve the faradaic efficiency of the C6 product. Initially, the working electrode morphology is changed to study the effects of increased electrochemical surface area of the electrode. Thus, nickel fibre felt and nickel foam are selected as working electrodes to be employed in the electrochemical cell, with the rest of the process parameters to be the same. As 1,3-butadiene and CO_2 compete to be absorbed on the nickel electrode surface for reduction, the porosity, surface roughness and increased electrochemical surface area with the same geometric surface area are considered for experimentation. With intermediate steps in increasing the ECSA of the nickel electrode, two sets of experiments are designed with the aim of studying the faradaic efficiency of the 3HDA product. The results and analysis of the experiments are

stated in the subsequent section 4.2.

4.2. Nickel Fibre Felt Cathode

Since the electrochemical surface area is increased in the nickel fibre felt electrode, the capacitive currents are high, which is observed in the cyclic voltammogram in Figure 4.5a. The green curve corresponding to CO_2 and 1,3-butadiene combined, observes a sharp surge in reduction current at -2 V, marking it as the onset potential. Additionally, the green curve almost coincides with the red curve, suggesting the mechanism to be dominated by the $CO_2^{\cdot-}$ radical anion attacking 1,3-butadiene, which is different to the mechanism observed in the nickel wire cathode. Beyond -2.5 V, the blank electrolyte solution also shows a sharp decrease in current, indicating the degradation of acetonitrile at higher potentials, which may yield unwanted side products.

The current densities for the nickel fibre felt electrode are calculated for the geometric area of 1 cm^2. The maximum diameter of nickel fibre felt pore is 30 μm, and the thickness is 0.4 mm and 82.5 % porosity. In Figure 4.5b, the chronoamperometry was performed at different potentials in the window from -2 V, i.e the onset potential, and -2.5 V, after which the electrolyte potentially begins to degrade. Considering the current densities calculated based on the geometric area, the current densities recorded for nickel fibre felt are comparatively lower than those for nickel wire. As observed in the cyclic voltammogram, the onset potential is shifted to -2 V from -2.4 V in the nickel wire cathode. This lowers the range of reduction potentials for conducting the CA tests, and hence lower current densities are observed.

For -2 V and -2.2 V, the current initially decreases and then forms a plateau at 3.5 $mA \cdot cm^{-2}$ and 7.5 $mA \cdot cm^{-2}$, respectively. The initial current decay indicates sluggish kinetics for activation, thus questioning the efficiency of the mechanism of $CO_2^{\cdot-}$ radical anion attacking 1,3-butadiene, with only a higher rate of CO_2 activation at the cathode. Conversely, at higher potential of -2.4 V, the current density is higher than that for -2.5 V, as the 1,3-butadiene reduction can be active at the cathode, referring to the CV in Figure 4.5a. Also, there is a surge in current indicating faster reaction kinetics initially and then a plateau. For the potential of -2.5 V, the current density is a plateau throughout the 120 minutes, indicating balanced reaction kinetics. The solid product is formed only in the CA test for -2.5 V, among the rest.

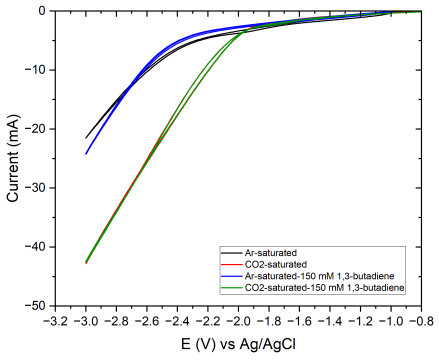

(a) Cyclic Voltammetry for nickel fibre felt and aluminium coil in acetonitrile and tetraethylammonium chloride electrolyte solution (200 mM) with (a) (black) blank electrolyte solution, (b) (red) CO_2 saturated electrolyte solution, (c) (blue) Argon deaerated and 1,3-butadiene added electrolyte solution (150mM), (d) (green) CO_2 saturated and 1,3-butadiene added electrolyte solution (150mM)

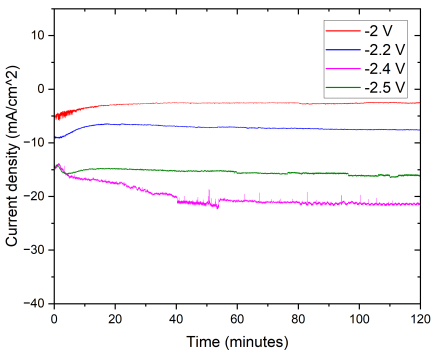

(b) Chronoamperometry experiments at potentials of (a) (red) -2 V vs Ag/AgCl, (b) (blue) -2.2 V vs Ag/AgCl,(c) (pink) -2.4 V vs Ag/AgCl,(d) (green) -2.5 V vs Ag/AgCl conducted for 120 minutes (on the x-axis) and the current density (on the y-axis), working electrode geometric area is 1 cm^2, 200 mM electrolyte solution of acetonitrile and tetraethylamonium chloride with CO_2 and 1,3-butadiene addition (150 mM)

Figure 4.5: (a) CV and (b) CA plots for acetonitrile and tetraethylammonium chloride with nickel fibre felt and aluminium coil as working and counter electrode, respectively

The faradaic efficiency, product distribution selectivity and yield lie in the range below 10 % as observed

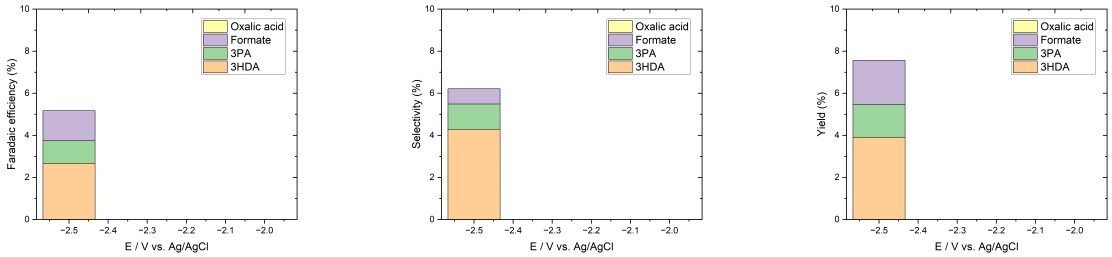

(a) Faradaic efficiency in '%' for products of the reaction at different potentials of CA experiments

(b) Selectivity in '%' for products of the reaction at different potentials of CA experiments

(c) Yield in '%' for products of the reaction at different potentials of chronoamperometry experiments

Figure 4.6: Faradaic efficiency, selectivity, and yield for products of the reaction at different potentials of the CA experiment for the nickel fibre felt working electrode

in Figure 4.6. Half of the combined faradaic efficiency is that of 3HDA, but the combined efficiency not even being 10 % indicates a lot of gaseous products are formed and HER is dominating at the cathode, thus forming a thick gas diffusion layer and reducing the active sites for CO_2 and butadiene reduction. The selectivity and yield of the 3HDA are more than 50 % of the product distribution among the carboxylated products, but are in a negligible amount for quantification, making it undesirable for an optimisation approach. If the current densities of nickel fibre felt are calculated for the relatively active sites, which are more than the geometric area and less than the electrochemical surface area, the current densities would be even smaller compared to the nickel wire. The proportionally lower current densities could indicate effective electron transfer for the synthesis of 3HDA product that would lead to higher faradaic efficiency, but is suppressed as the competing gas evolution reactions are active which cause mass transfer limitations. The result reflects that increasing the electrochemical surface area by changing the electrode surface morphology does not improve the product efficiency and selectivity.

4.3. Nickel Foam Cathode

Since the electrochemical surface area is further increased in the nickel foam electrode, the capacitive currents are even higher, which is observed in the cyclic voltammogram in Figure 4.7a. The green curve corresponding to CO_2 and 1,3-butadiene presence, observes a sharp surge in reduction current at -2.4 V, marking it as the onset potential. Additionally, the green curve almost coincides with the blue curve, suggesting the mechanism to be dominated by the butadiene radical anion attacking CO_2 , which is similar to the mechanism observed in the nickel wire cathode, and different from the mechanism for nickel fibre felt. Beyond -2.75 V, the blank electrolyte solution also shows a sharp decrease in current, indicating the activity of acetonitrile reduction at higher potentials, which may yield unwanted side products. In this case, the chronoamperometry experiments are conducted for a range of potentials between -2.2 V to -2.7 V, that is, potentials higher and lower than the onset potential. The CA tests are performed for lower potential because of the CO_2 curve having a reduction potential lower than the green curve of CO_2 and 1,3-butadiene.

For chronoamperometry tests, the curve for -2.4 V potential shows decay in current initially, suggesting sluggish kinetics, whereas the other curves show an increase in current initially and then a plateau, which suggests faster kinetics. The current densities are calculated based on the geometric area of 1 cm^2 and are thus comparable to the current densities observed for nickel wire electrode. The nickel foam is 4mm in thickness. The vast difference in current densities at higher potential suggests that there is a large number of active sites, as the higher current is faradaic in nature. Chronoamperometry experiments are conducted at -2.2 V, -2.4 V, -2.6 V and -2.7 V.

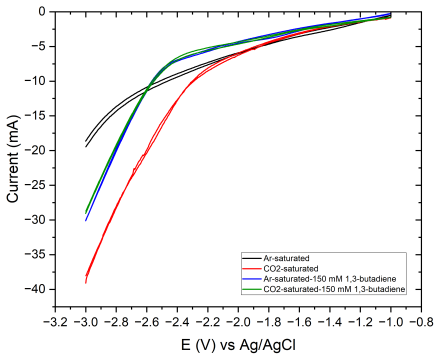

(a) Cyclic Voltammetry for nickel foam and aluminium coil in acetonitrile and tetraethylammonium chloride electrolyte solution (200 mM) with (a) (black) blank electrolyte solution, (b) (red) CO_2 saturated electrolyte solution, (c) (blue) Argon deaerated and 1,3-butadiene added electrolyte solution (150mM), (d) (green) CO_2 saturated and 1,3-butadiene added electrolyte solution (150mM)

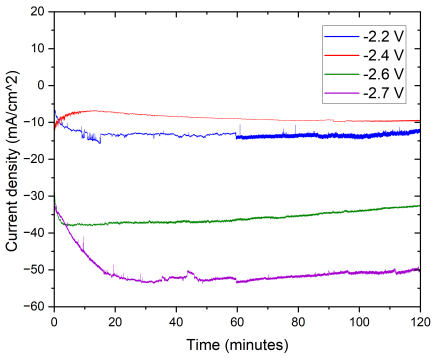

(b) Chronoamperometry experiments at potentials of (a) (blue) -2.2 V vs Ag/AgCl, (b) (red) -2.4 V vs Ag/AgCl,(c) (green) -2.6 V vs Ag/AgCl,(d) (purple) -2.7 V vs Ag/AgCl conducted for 120 minutes (on the x-axis) and the current density (on the y-axis), working electrode geometric area is 1 cm^2, 200 mM electrolyte solution of acetonitrile and tetraethylamonium chloride with CO_2 and 1,3-butadiene addition (150 mM)

Figure 4.7: (a) CV and (b) CA plots for acetonitrile and tetraethylammonium chloride with nickel foam and aluminium coil as working and counter electrode, respectively

The highest faradaic efficiency is observed for the reduction potential of -2.4 V, which is the onset potential, and there is no solid product formation at -2.6 V as seen in Figure 4.8a. There is no trend observed for the products in these CA experiments. At -2.2 V reduction potential only 3HDA product is formed and no formate, oxalic acid or 3PA, this suggests that although in minimal quantity the C6 product has 100% selectivity at lower potential than the onset potential for nickel foam cathode as observed in Figure 4.8b. The selectivity rises from -2.2 V to -2.7 V for the 3HDA product, while the product distribution for other products remains similar at -2.4 V and -2.7 V. Although the faradaic efficiency of 3HDA is maximum at -2.4 V and very negligible at -2.7 V, suggesting that at higher potentials, when the electrode passivation is possible, side reactions dominate. The yield of the products show a similar trend to that of the selectivity graph. Since the faradaic efficiency for 3HDA is not appreciable even at -2.4 V, the optimisation effort is not considered to be fruitful. Similar arguements of gas evolution reaction due to enhanced electrochemical suraface area remain as a primary factor to obsrtuct CO_2 and 1,3-butadiene reduction at the cathode. For better performance towards product formation, the nickel foam electrode needs to be properly cleaned and etched before use for having NiOOH layer formed which is electrochemically more active and provides a higher electrochemical surface area than bare nickel foam. This can possibly increase the faradaic efficiency for 3HDA.

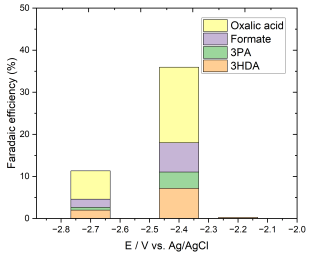

(a) Faradaic efficiency in '%' for products of the reaction at different potentials of CA experiments

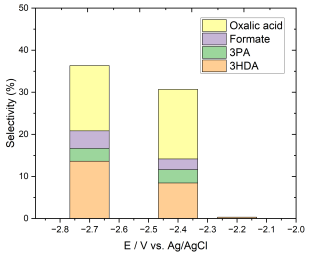

(b) Selectivity in '%' for products of the reaction at different potentials of CA experiments

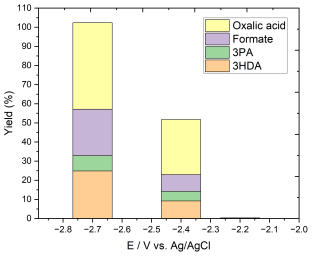

(c) Yield in '%' for products of the reaction at different potentials of chronoamperometry experiments

Figure 4.8: Faradaic efficiency, selectivity, and yield for products of the reaction at different potentials of the CA experiment for the nickel foam working electrode

As a side note, formate synthesis is only observed for nickel foam and nickel wire cathode and not for

nickel fibre felt cathode. For nickel foam and nickel wire cathode, the plausible reaction mechanism follows simultaneous attack of butadiene radical anion and $CO_2^{\cdot-}$ radical anion, and for nickel fibre felt cathode experiments, the plausible reaction mechanism follows the attack of $CO_2^{\cdot-}$ radical anion on 1,3-butadiene. Thus, a plausible effect of formate synthesis can be associated with the H^+ ion released by reduction of 1,3-butadiene to the butadiene radical anion at the cathode, since the moisture content in the electrolyte for these three set of experiments remains the same.

Once the nickel electrode morphologies are studied for the undivided electrochemical cell, the electrode material is changed to study the product formation and subsequently the faradaic efficiency.

4.4. Copper Wire Cathode

Copper is one of the favoured electrodes in the electrochemical reduction of CO_2. Additionally, it has been reported to produce considerable efficiency of 29.5% and 60% yield by Li et al. [23]. There is further scope for optimisation based on copper electrodes in the electrochemical reduction of CO_2, if the preliminary experiment yields good results. Since higher water content in acetonitrile leads to excessive HER, when copper electrodes are employed, dry acetonitrile and tetraethylammonium chloride electrolyte is used [9]. Before the reaction, the copper electrodes are activated and electropolished by the method drafted by Asvin et al. [20] and the procedure is written in the subsection 3.4.1.

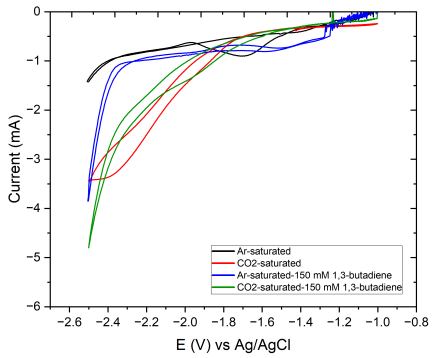

(a) Cyclic Voltammetry for copper wire and aluminium coil in acetonitrile and tetraethylammonium chloride electrolyte solution (200 mM) with (a) (black) blank electrolyte solution, (b) (red) CO_2 saturated electrolyte solution, (c) (blue) Argon deaerated and 1,3-butadiene added electrolyte solution (150mM), (d) (green) CO_2 saturated and 1,3-butadiene added electrolyte solution (150mM)

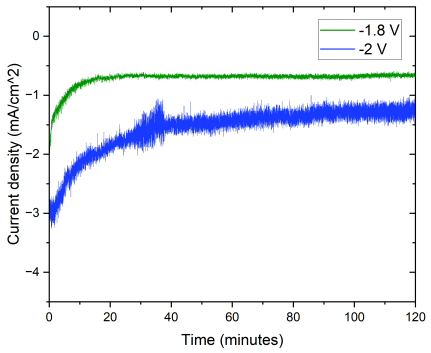

(b) Chronoamperometry experiments at potentials of (a) (green) -1.8 V vs Ag/AgCl, (b) (blue) -2 V vs Ag/AgCl, about the onset potential observed from the cyclic voltammogram, conducted for 120 minutes (on the x-axis) and the current density (on the y-axis), working electrode area is 1 cm^2, 200 mM electrolyte solution of acetonitrile and tetraethylamonium chloride with CO_2 and 1,3-butadiene addition (150 mM)

Figure 4.9: (a) CV and (b) CA plots for acetonitrile and tetraethylammonium chloride with copper wire and aluminium coil as working and counter electrode, respectively

The cyclic voltammetry is performed between -1 V and -2.5 V. In the CV, the green curve shows a sharp increase in current at -1.8 V, marking it as the onset potential. The reduction potential of the red curve, which is CO_2 saturated, is the same as the green curve, focusing on the mechanism proceeding via $CO_2^{\cdot-}$ radical anion attack on 1,3-butadiene. Beyond -2.4 V, the blank electrolyte degrades as the current increases. Thus, chronoamperometry is performed for the onset potential of -1.8 V and a higher potential of 2 V.

The current densities for copper wire working electrode are significantly lower than those for nickel wire. For the onset potential of -1.8 V, the current density is around 700 $\mu A \cdot cm^{-2}$, and that for -2 V is about 1.3 $mA \cdot cm^{-2}$. The CA curves observe decay in current initially and then a plateau that suggests sluggish reaction kinetics at the cathode, indicating mass transfer limitations. Minimal solid product of 1 mg was formed at -1.8 V, and no product was formed at -2 V. Within the limited solid product formed, all of it was formate. Since formate is the only product formed, the cathode acts as an electrocatalyst

for CO_2 reduction, but the reaction is not proceeding via the attack on 1,3-butadiene to form C5 or C6 products.

4.5. Controlled Water Content in Electrolyte

Another major issue in product formation from the first set of experiments using nickel cathode is the generation of higher amounts of formates and oxalic acid as side products. Formates are formed when the $CO_2^{\cdot-}$ radical anion is protonated with H^+ ions [12], and oxalates are formed when the $CO_2^{\cdot-}$ radical anions couple to form a dimer [5]. As the electrolyser environment is initially saturated and then bubbled with CO_2 during the reaction for a sufficient amount of CO_2 to be reduced at the cathode, at every point there is excess which leads to side products. The protonation is mainly linked to the amount of water present in the electrolyte solution. The supporting electrolyte of tetraethylammonium chloride is highly hygroscopic in nature, allowing it to attract moisture in the electrolyte solution, even after overnight drying in an oven. To suppress this issue, dry acetonitrile is used, which intrinsically reduces the water content from about 250 ppm to 100 ppm before the electrolyte solution is made with tetraethylammonium chloride. The water content in the electrolyte is measured using the Karl Fischer Titration in the laboratory. After making the electrolyte solution of dry acetonitrile and tetraethylammonium chloride, the water content is measured again upon CO_2 saturation, which is between the range of 150 to 200 ppm. This is significantly lower than the range of 350 to 400 ppm water content that is recorded in acetonitrile and tetraethylammonium chloride electrolyte solution, making the water content about half. With an aim to suppress the side products and observe the product distribution [24], this measure is taken. Since the best performance among the nickel electrode morphologies was given by nickel wire, it was chosen as the working electrode for the set of experiments. Referring to the faradaic efficiency, product selectivity and the yield in Figure 4.2, it was best suited to carry reactions in the window of -2.5 V to -2.7 V.

The chronoamperometry experiments were thus carried out at -2.5 V, -2.6 V and -2.7 V as observed in Figure 4.10. The current density for -2.7 V in the experiment is higher by 10 $mA \cdot cm^2$, but for the rest of the reduction potentials, it is in a similar range. All the current densities show a similar trend where the current increases with time, showing faster kinetics, but the current does not plateau at any point showing potential window for the current to further decrease with time.

No quantifiable solid product is formed at the reduction potential of -2.5 V. Maximum combined faradaic efficiency is observed at -2.6 V, followed by that for -2.7 V as seen in Figure 4.11a. Although most of the faradaic efficiency goes to formate at -2.6 V, the faradaic efficiency for 3HDA is more than twice at -2.6 V compared to -2.7 V. The selectivity of 3HDA product is similar at both reduction potentials as observed in Figure 4.11b. The yield for 3HDA is in the range of 5 to 10 % for both reduction potentials, as observed in Figure 4.11c. Since the faradic efficiency and selectivity of the C6 product are highest at -2.6 V, and the same was observed for the first experimental set-up with acetonitrile, thus making it an ideal choice of reduction potential to test the impact of water content on the products formed.

Additionally, to comment on the oxalic acid and formates, they are quite suppressed at lower water content in the electrolyte, but at -2.6 V there is still a lot of faradaic efficiency going to formate product. This could also be the H^+ ion from the reduced 1,3-butadiene, as the reaction mechanism follows butadiene radical anion attack on CO_2. Furthermore, there is no production of 3PA when dry acetonitrile is used as an electrolyte, suggesting dicarboxylation completion reaction in the environment.

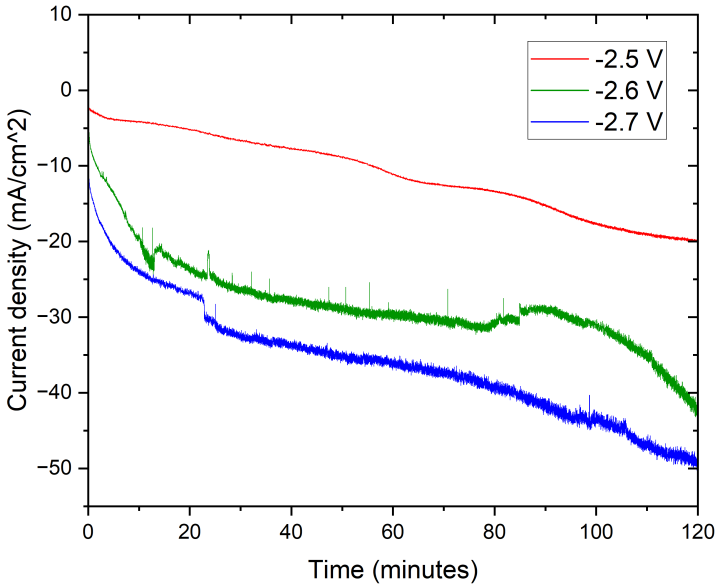

Figure 4.10: Chronoamperometry experiments at potentials of (a) (red) -2.5 V vs Ag/AgCl, (b) (green) -2.6 V vs Ag/AgCl,(c) (blue) -2.7 V vs Ag/AgCl conducted for 120 minutes (on the x-axis) and the current density (on the y-axis), working electrode area is 0.32 cm^2, 200 mM electrolyte solution of acetonitrile and tetraethylamonium chloride with CO2 and 1,3-butadiene addition (150 mM) and water content between 150 to 200 ppm

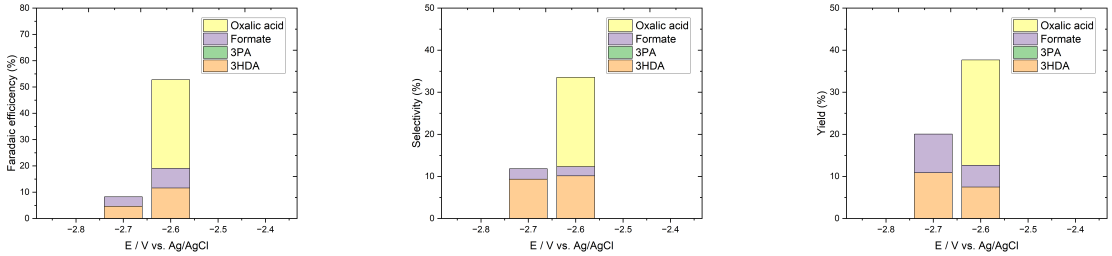

(a) Faradaic efficiency in '%' for products of the reaction at different potentials of CA experiments

(b) Selectivity in '%' for products of the reaction at different potentials of CA experiments

(c) Yield in '%' for products of the reaction at different potentials of chronoamperometry experiments

Figure 4.11: Faradaic efficiency, selectivity, and yield for products of the reaction at different potentials of the CA experiment for the nickel wire working electrode with controlled water content in the electrolyte

Furthermore, to test the effects of the presence of water on the faradaic efficiency, product distribution and other factors, experiments are conducted with controlled addition of water to the dry acetonitrile and tetraethylammonium chloride electrolyte solution in controlled measure of volume percentages to study the trend. The results and analyses for the same are mentioned in the subsequent section 4.6.

4.6. Water Addition to Electrolyte

As water content effects need to be measured for product selectivity and faradaic efficiency of the 3HDA product and subsequent surge or decrease of other products, the chronoamperometry experiments are performed at -2.6 V reduction potential. The conditions considered for the study are a deaerated electrolyte solution using argon before CO_2 saturation, dry acetonitrile electrolyte (from a previous set of experiments), 0.01% v/v addition of water, 0.5% v/v addition of water and 1% v/v addition of water. The current densities for dry acetonitrile and water added electrolyte are in a similar range, between 42 $mA \cdot cm^{-2}$ to 48 $mA \cdot cm^{-2}$. The deaerated dry acetonitrile has significantly lower current density, which

suggests that the trace impurities may affect the excess current densities or might be causing excess capacitive current during the reaction. The CA curves have an initial surge in the current, explaining faster kinetics and the later plateau over the duration of the reaction that the conditions lead to stability.

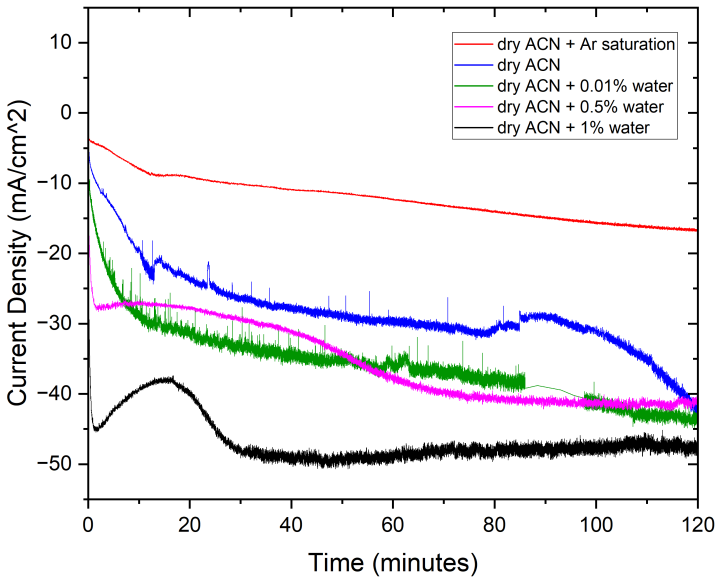

Figure 4.12: Chronoamperometry experiments at -2.6 V vs Ag/AgCl potentials for (a) (red) Argon deaerated electrolyte solution of dry ACN, (b) (blue) electrolyte solution of dry ACN,(c) (green) 0.01% v/v water added electrolyte solution of dry ACN, (d) (pink) 0.5% v/v water added electrolyte solution of dry ACN, (e) (black) 1% v/v water added electrolyte solution of dry ACN for 120 minutes (on the x-axis) and the current density (on the y-axis), working electrode area is 0.32 cm^2, 200 mM tetraethylamonium chloride in dry acetonitrile with CO_2 and 1,3-butadiene addition(150 mM)

The combined faradaic efficiency and the faradaic efficiency for 3HDA both show a decrease in trend as the water content increases, as seen in Figure 4.13a . With the increase in water content, the amount of oxalic acid and formate also shows a steady decline, underpinning that the prominent HER and thick gas diffusion layer formation resist the electroreduction of CO_2 at the cathode surface after a certain duration of reaction. At 1 % v/v water addition, the faradaic efficiency is only for 3HDA, which is below 1 %. Also, a remarkable result is that there is negligible (unquantifiable by HPLC analysis) 3PA formed in any of the experiments, indicating efficient dicarboxylation.

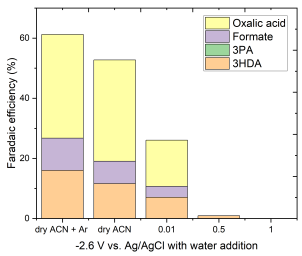

(a) Faradaic efficiency in '%' for products of the reaction at -2.6 V potential for varied water content in %

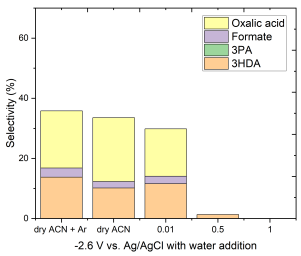

(b) Selectivity in '%' for products of the reaction at -2.6 V potential for varied water content in %

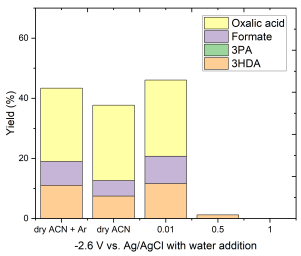

(c) Yield in '%' for products of the reaction at -2.6 V potential for varied water content from 0.01% to 1%

Figure 4.13: Faradaic efficiency, selectivity, and yield for products of the reaction at -2.6 V potential of the CA experiment for the nickel wire working electrode with controlled water content and water addition from 0.01% to 1% in the electrolyte

The selectivity of C6 product remains quite uniform for deaerated electrolyte, normal electrolyte conditions and 0.01% v/v water addition, implying that the selectivity of the product is not affected by water content varying between 150 ppm to 400 ppm. Since there is only 3HDA formed at higher water content in the electrolyte, the selectivity is 100 % for the product as seen in Figure 4.13b. The yield shows a similar trend to that of selectivity as seen in Figure 4.13c. The yield for 3HDA lies in the range of 8 to 10 % for deaerated electrolyte, normal electrolyte conditions and 0.01% v/v water addition, and subsequently decreases with the increase in water content.

4.7. Temperature Variation

Li et al. have explored the effects of increasing the temperature for process conditions in the electroreduction of 3HDA to adipic acid, i.e the hydrogenation step [23]. Taking inspiration, preliminary experiments are performed to study the effect of increased temperature on the product selectivity and faradaic efficiency. According to the results of Li et al., the yield and faradaic efficiency both increased almost threefold between 20°C and 60°C.

Since the best faradaic efficiency and selectivity for 3HDA product is observed in the first set of experiments with nickel wire electrode and aluminium coil in acetonitrile and tetraethylammonium chloride, it is selected to study the effect on product distribution and faradaic efficiency with increasing temperature. Hence, the chronoamperometry experiments are performed at 40°C and 60°C, with error of +/- 1°C, as seen in Figure 4.14. In the initial set of experiments, maximum faradaic efficiency was achieved at -2.4 V, and since the temperature variation experiment is preliminary, the increase in faradaic efficiency is to be studied to understand the direct effect of temperature. The current densities increase at higher temperatures, indicating that the conductivity inside the cell increases. Additionally, the CA curves observe an initial increase in current, suggesting faster reaction kinetics. The surge in current at 60°C is so significant, indicating that the kinetics of the reaction are boosted with better conductivity of the electrolyte. The excessive noise in the CA curve at 60°C is due to the excess conductivity of the electrolyte, as there is over-reduction at the cathode. Over-reduction is the excess current drawn for the same potential due to improved conductivity and thus flooding the cathode with unwanted reduction and thus excess gaseous product formation. The improved rate of reaction can be inferred from the data on the reaction completion time for the CA test for temperature variation. The reaction completion time at 20°C is 37.8 hours, at 40°C it is 23.8 hours and at 60°C it is 20.4 hours. The time for completion of the reaction is calculated based on the formulae mentioned in Appendix A.1.

The combined faradaic efficiency decreases drastically as the temperature increases, and the same trend is observed for the faradaic efficiency of 3HDA in Figure 4.15a. Additionally, formate is only synthesised at room temperature, and oxalic acid is synthesised at room temperature and 40°C, which is much lower in faradaic efficiency than at room temperature. Selectivity of products in Figure 4.15b and yield of products in Figure 4.15c show the same trend. Selectivity of 3HDA drops from about 10% at room temperature to 3% at 60°C. The yield for 3HDA is around 3% at 40°C and 60°C as well. 3PA is not formed as a product in solid form at 40°C and 60°C, and it is hence not seen in any of the subfigures of Figure 4.15. Thus, the minimal monocarboxylation product of C5 at room temperature is completely suppressed at higher temperatures, providing 100% for the C6 product at higher temperatures. Other side products are also suppressed at higher temperatures, as the elevated temperature might destabilise the intermediates that are formed for oxalic acid dimerisation from CO_2^- radical anion. Also, at higher temperatures, since the fardaic efficiency decreases even after improved kinetics, the 3HDA dissolved in the supernatant needs to be checked.

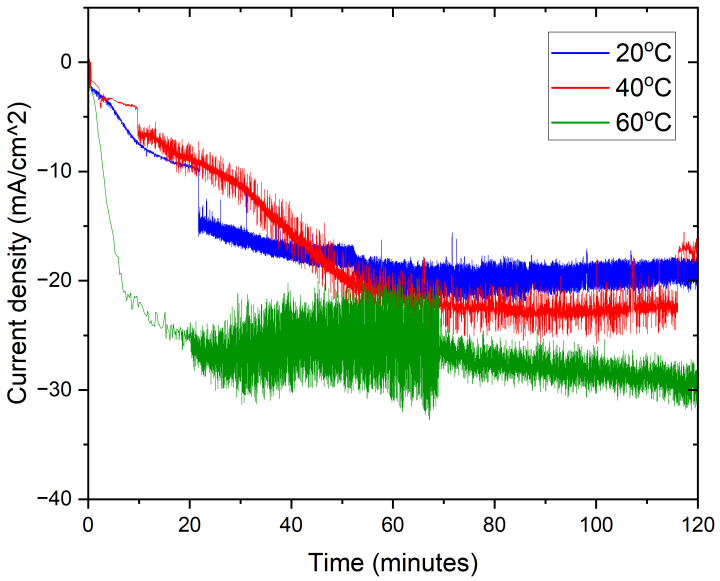

Figure 4.14: Chronoamperometry experiments at -2.4 V vs Ag/AgCl potentials for (a) (blue) room temperature conditions at 20°C, (b) (red) 40°C,(c) (green) 60°C for 120 minutes (on the x-axis) and the current density (on the y-axis), working electrode area is 0.32 cm^2, 200 mM tetraethylamonium chloride in acetonitrile with CO_2 and 1,3-butadiene addition(150 mM)

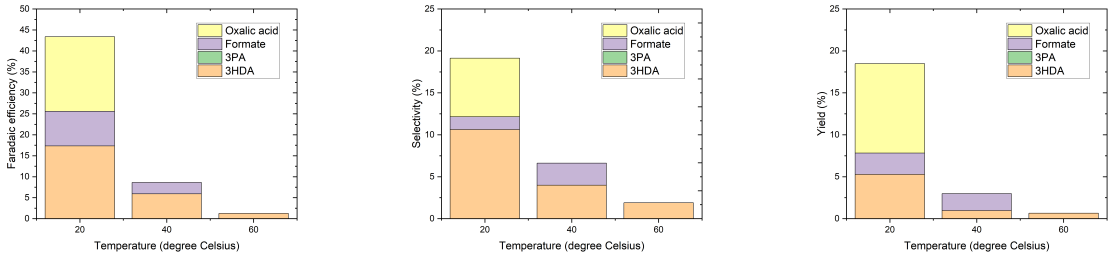

(a) Faradaic efficiency in '%' for products of the reaction at -2.4 V potential for different temperatures

(b) Selectivity in '%' for products of the reaction at -2.4 V potential for different temperatures

(c) Yield in '%' for products of the reaction at -2.4 V potential for different temperatures of 40°C and 60°C

Figure 4.15: Faradaic efficiency, selectivity, and yield for products of the reaction at -2.4 V potential of the CA experiment for the nickel wire working electrode at different temperatures of 20°C, 40°C and 60°C

4.7.1. Solubility of products in supernatant

The faradaic efficiency of products decreased for 3HDA as temperature was increased in the temperature variation experiment. Thus, at higher temperatures, suggesting that the product may be dissolved in the supernatant. To check the dissolved supernatant solubility, tests were performed for the 3HDA product in the supernatant using Crystal16. Samples were made for three concentrations of 10 mM, 15 mM, and 20 mM, and by weight percentage, it translates to 2.6 mg, 3.7 mg and 4.9 mg of 3HDA, respectively, in 1.8 ml of acetonitrile and tetraethylammonium chloride electrolyte. The method of finding the temperature for complete solubility of a product in a solvent is given in the section 3.3.4. The data for the solubility temperature with the standard deviation or error is seen in Table 4.1.

This data provides a ballpark of the maximum amount of 3HDA that could be dissolved in the supernatant at room temperature is less than or equal to 10 mM. Further to investigate the dissolved 3HDA in the supernatant, absorption and separation techniques are used. Since water is more protic in nature than acetonitrile, it can be used for extracting 3HDA from the supernatant. The 3HDA absorption is

Table 4.1: Solubility temperatures for concentrations of 3HDA in acetonitrile and TEACl

Concentration of 3HDA (mM)	Solubility temperature (°C)	Standard deviation in temperature
10	23.15	0.55
15	29.975	0.225
20	33.85	0.15

done using 2 ml of supernatant and 2 ml of 0.5 M NaOH (HPLC eluent). Since the volumes are in the ratio of 1:1, the suspension is thoroughly mixed before being allowed to stand for a couple of hours. Once the layers are separated, the upper layer of supernatant is taken out. The separation is not absolute in 1:1 ratio but rather in an approximate ratio of 2.75:1.25, in which 2.75 ml is the water-dominated layer. The separation is performed as the supernatant can not be directly tested in the HPLC, as the column is sensitive and the organic matrix can disrupt the elution process. The collected sample is analysed in HPLC. The quantity was then extrapolated for the 37 ml of supernatant on average, and the faradaic efficiency of the dissolved 3HDA product is 0.67% at 40°C and 2.33% at 60°C, which is negligible. Subsequently, the faradaic efficiency of the 3HDA in supernatant for the chronoamperometry test at room temperature was also performed and it was calculated to be 0.68%. The faradaic efficiency increase for the product after analysing the supernatant is seen in Figure 4.16.

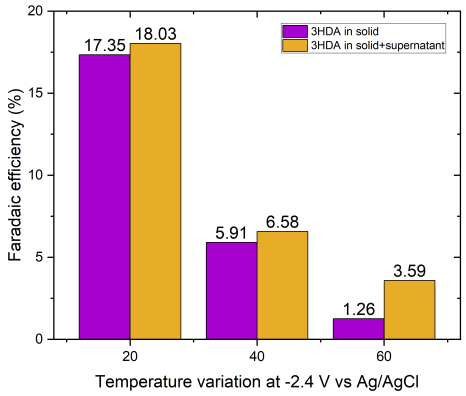

Figure 4.16: The comparison of the fardaic efficiency (%) of 3DHA in solid sample and the solid sample and supernatant combined

Similarly, to study the 3PA product dissolved in the supernatant, the calibration of 3PA is done for Liquid GC, and a peak is identified around 14.4 minutes for an hour of cycle. Subsequently, the calibration curve is plotted, referred to in the Appendix A.6. The supernatant is compatible with the Liquid GC, hence it can be directly checked for dissolved 3PA product. After the analysis, no 3PA product was found in the supernatant. For all the analysis, fresh supernatant is used.

4.7.2. Unreacted 1,3-butadiene in Supernatant

Checking the unreacted 1,3-butadiene in the supernatant is of key importance as well. The caution to be practised for testing the unreacted 1,3-butadiene is that the supernatant needs to be examined right after the centrifugal separation. Keeping the supernatant standing for a longer time after separation allows dimerisation or polymerisation of butadiene with other hydrocarbons in the organic matrix. Once the fresh supernatant is checked for unreacted butadiene, the conversion percentage during the reaction time can be confirmed. Also, the mass balance for the reaction products can be done for the reacted butadiene, instead of extrapolating the products for the completion time of the reaction. The yield of 3HDA can be calculated for the reaction time duration and can be compared to the yield of the

completed reaction to comment on uniform reaction behaviour and stability of current density.

As discussed in the methodology, the electrochemical set-up has 150 mM of 1,3-butadiene, which takes more than 2 hours of reaction time for complete conversion. Thus, accounting for the unreacted 1,3-butadiene at the end of 2 hours of reaction is important. This helps to make the material balance calculations. A fresh supernatant solution was analysed in Liquid GC, and using the calibration curve A.5, the unreacted 1,3-butadiene was measured as 110 mM out of the 150 mM. The conversion of 1,3-butadiene in this case is approximately 26%. The yield for the reaction is about 8% , which is the same as that found from the extrapolation of the product for completion of the reaction, underpinning the accuracy of the extrapolated product results for the reaction.

4.8. Supporting Electrolyte Variation

After the optimisation strategies based on electrode morphology, electrode material, electrolyte water content control and increasing temperature, the supporting electrolytes are varied in order to study the effect of improved selection of the C6 product. This optimisation step is inspired by the research of Yuan et al., who studied the influence of supporting electrolytes on the activation process of CO_2 apart from the conductivity function [41].

As mentioned in Table 2.2, the use of different supporting electrolytes can improve the selectivity and yield. Thus, keeping the rest of the conditions the same, the supporting electrolytes tetrabutylammonium tetrafluoroborate (TBABF4) and tetrabutylammonium hexafluorophosphate (TBAPF6) are employed to study the effect of supporting electrolytes on the faradaic efficiency and selectivity of 3HDA.

The electrochemical reactions do not proceed and show an error of 'amplifier overload potential' within seconds or the first few minutes of running either CV or CA experiments. The concentration of supporting electrolytes in the electrolyte solution was kept at 200 mM, the same as that of TEACl. A set of experiments was planned with the increased TBAPF6 concentration for 500 mM in the electrolyte solution, which resulted in the same overload stoppage, although the conductivity increased to 13.54 mS/cm for increased concentration of the supporting electrolyte. Hence, the conductivity of the electrolyte solutions at 200 mM concentration was checked and mentioned in Table 4.2.

Table 4.2: Conductivity of supporting electrolytes

Supporting electrolyte	Conductivity (mS/cm)
TEACl	7.8
TBABF4	8.45
TBAPF6	8.05

Since the conductivities for $TBABF_4$ and $TBAPF_6$ lie in the same ballpark as TEACl, the problem for BF_4^- and PF_6^- passivating the working electrode was checked by Scanning Electron Microscopy (SEM). The report for the same is attached in Appendix A.4. The phosphorus content on the working electrode wire is signalled to be negligible, and no traces of fluorine are found, thus barring the possibility of passivation of the electrode due to the ion deposition at the cathode. Thus leaving with the logic that the BF_4^- and PF_6^- ions are larger in size, and hence the mobility of these ions in an undivided cell is less, leading to amplifier overload issues in running the experiments.

5

Conclusion

This thesis presents an in-depth experimental exploration of the electrochemical dicarboxylation of 1,3-butadiene with captured CO_2 to synthesise 3HDA, a crucial precursor for adipic acid. The research has successfully demonstrated that by employing a nickel wire working electrode in a sealed, undivided electrochemical cell with acetonitrile and tetraethylammonium chloride (TEACl) as the electrolyte solution, the electroreduction of CO_2 and 1,3-butadiene can be achieved with notable selectivity and efficiency towards the desired C6 product.

Through comprehensive cyclic voltammetry and chronoamperometry experiments, the onset and optimal reduction potentials were identified. The maximum faradaic efficiency and product selectivity for 3HDA were observed for a reduction potential of –2.6 V vs Ag/AgCl. At -2.6 V, the 3HDA faradaic efficiency is 14% and a 100% selectivity of 3HDA among the carboxylation products is achieved. 3PA is not synthesised at -2.6 V, thus identifying that the reaction favours dicarboxylation.

The study also confirmed that nickel wire outperforms other morphologies like nickel fibre felt and foam for the faradaic efficiency achieved for 3HDA, which is below 10%, primarily due to its catalytic surface characteristics, stability and reaction kinetics compatibility. The current densities are lower for nickel fibre and foam cathodes, and most of the charge is consumed for the synthesis of gaseous products, predominantly hydrogen, at the cathode. This forms a thicker gas diffusion layer, resisting the efficient CO_2 reduction at the cathode.

Furthermore, for the electrolysis, employing a copper wire electrode does not yield a quantifiable solid product, and the minimal solid product synthesised is formate. Thus, indicating that CO_2 is reduced in limited quantity but does not proceed with a nucleophilic attack on 1,3-butadiene.

Further, optimising process parameters revealed that moisture content in the electrolyte plays a role in selectivity. Using dry acetonitrile had a moderate impact on the faradaic efficiency of 3HDA at -2.6 V. There was no 3PA synthesis for any of the reduction potentials when dry acetonitrile was used as an electrolyte. The incremental water additions suppressed overall faradaic efficiency, although not linearly. Since the reactions with water control were carried out at -2.6 V, the 3PA (monocarboxylated product) formation was suppressed. Additionally, the graph showed a decrease in 3HDA faradaic efficiency with the increasing water content.

Interestingly, increasing temperature enhanced reaction rate but led to a decline in solid product quantification, potentially due to increased product solubility in the supernatant, as corroborated by solubility analysis using Crystal16. The faradaic efficiency of the dissolved 3HDA was calculated, and even after that, the faradaic efficiency for 3HDA at 40°C was 6.58% and for 60°C it was 3.59%.

The investigation into alternative supporting electrolytes, such as $TBABF_4$ and $TBAPF_6$ was inconclusive due to operational challenges. Finally, the experiments underscore that achieving higher 3HDA faradaic efficiency hinges on minimising HER, tuning moisture content in the electrolyte, and selecting appropriate electrode materials and cell conditions.

In conclusion, this work provides a strong foundation for sustainable 3HDA production via CO_2 utilisation, supports the transition to renewable-based chemical synthesis, and shows a pathway for future scale-up efforts by addressing critical bottlenecks in electrode design, electrolyte formulation, and cell operation.

6

Recommendation for Future Research

This thesis provides a promising experimental foundation for the electrochemical dicarboxylation of 1,3-butadiene with captured CO_2 to synthesise 3-hexene-1,6-dioic acid (3HDA). However, further research is needed to refine the process, improve faradaic efficiency, and enhance selectivity towards the desired product.

While nickel wire outperformed other morphologies in this study, the low faradaic efficiencies observed with nickel fibre felt and nickel foam cathode highlight the need for further surface treatment or activation. Future studies should investigate electrochemical roughening, surface etching, or NiOOH formation for nickel foam to enhance catalytic activity and suppress hydrogen evolution.

The formation of side products such as formate and oxalic acid can be partially attributed to water content and CO_2 over-reduction at the cathode. Dry acetonitrile use decreases the moisture content in the electrolyte to 150 ppm, whereas measures can be taken, like electrolyte preparation in an inert environment, to decrease the water content to about 50 ppm. This will provide a strong reflection on the effect of suppressed HER and synthesis of oxalic acid and formate on the faradaic efficiency gained by 3HDA.

Nickel wire was a promising cathode for the thesis, emphasising the importance of cathode selection. The surface morphology is instrumental to be studied in depth by material scientists to explore techniques like doping the electrodes or employing a bi-metallic electrode like Ni-Cu for improving the controlled synthesis of 3HDA. Every electrode morphology and material shows a different plausible mechanism on gauging their cyclic voltammograms. The two mechanisms for the first carboxylation step may have different effects on the final product formation and the product distribution. Thus, studying the reaction intermediates in the gas diffusion layer using in situ spectroscopy techniques would bring clarity to the preferred mechanism for dicarboxylation. Additionally, a greater area of nickel wire can also be used to be employed in the existing electrochemical setup to study the faradaic efficiency and product distribution, which is affected by the increased geometric surface area.

Most exemplary results mentioned in the literature for the electrocarboxylation of dienes are gained by the pressure inlet of CO_2. CO_2 has better solubility in the organic electrolyte solvents at higher pressure and alters the boundary regime of the cathode surface to enhance the CO_2 reduction to CO_2^{-} radical anion, and subsequently allows better reaction dynamics. Using an undivided cell which can withstand high pressures up to 3 or 4 MPa would be ideal.

References

[1] Statistics Netherlands (CBS). *CO_2 equivalents*. Accessed: 2025-04-06. 2019. URL: https://www.cbs.nl/en-gb/news/2019/37/greenhouse-gas-emissions-down/co2-equivalents.

[2] Agilent Technologies. *Analysis of Gas Samples Using the Agilent 490 Micro GC*. Tech. rep. 5991-1499EN. Accessed: 2025-06-10. Agilent Technologies, 2012. URL: https://www.agilent.com/cs/library/applications/5991-1499EN.pdf.

[3] Agilent Technologies. *Fast, Reliable Natural Gas and Natural Gas Liquids (NGL) Analysis with the Agilent 490 Micro GC*. Tech. rep. 5991-5515EN. Accessed: 2025-06-10. Agilent Technologies, 2015. URL: https://www.agilent.com/cs/library/applications/5991-5515EN.pdf.

[4] Alphalyse. *How to Identify Peaks Observed by UV-HPLC in Stability Studies*. Accessed: 2025-06-10. n.d. URL: https://alphalyse.com/how-to-identify-peaks-observed-by-uv-hplc-in-stability-studies/.

[5] Vera Boor et al. "Electrochemical Reduction of CO□ to Oxalic Acid: Experiments, Process Modeling, and Economics". In: *Industrial & Engineering Chemistry Research* 61.40 (2022), pp. 14837–14846. DOI: 10.1021/acs.iecr.2c02647. URL: https://doi.org/10.1021/acs.iecr.2c02647.

[6] J. Bringmann and E. Dinjus. "Electrochemical synthesis of carboxylic acids from alkenes using various nickel-organic mediators: CO2 as C1-synthon". In: *Applied Organometallic Chemistry* 15.2 (2001), pp. 135–140. DOI: 10.1002/1099-0739(200102)15:2<135::AID-AOC108>3.0.CO;2-L.

[7] D. F. Bruggeman, M. Zwart, and A. C. Garcia. "Tailoring Electrocarboxylation Pathways on Lead Cathodes: Insights into Electrolysis Mode". In: *ChemElectroChem* 12.4 (2025), e202400580. DOI: 10.1002/celc.202400580. URL: https://doi.org/10.1002/celc.202400580.

[8] The Chemical Company. *ADI-PURE® Adipic Acid by Invista*. Accessed: 2025-04-06. 2025. URL: https://thechemco2.wpengine.com/chemical/adi-pure-adipic-acid-invista/.

[9] Connor Deacon-Price et al. "Influence of Water Content on Electrochemical CO_2 Reduction in Acetonitrile Solution on Cu Electrodes". In: *ChemCatChem* 17.6 (2025), e202401332. DOI: 10.1002/cctc.202401332. URL: https://doi.org/10.1002/cctc.202401332.

[10] Connor Deacon-Price et al. "The Effect of the Tetraalkylammonium Cation in the Electrochemical CO_2 Reduction Reaction on Copper Electrode". In: *ACS Catalysis* 14.17 (2024), pp. 12928–12939. DOI: 10.1021/acscatal.4c02297. URL: https://doi.org/10.1021/acscatal.4c02297.

[11] DEK Research. *Sealed Electrochemical Cell 50 mL – 3120*. Accessed: 2025-06-10. n.d. URL: https://www.dekresearch.com/sealed-electrochemical-cell-50ml-3120.html.

[12] Dina Ewis et al. "Electrochemical reduction of CO_2 into formate/formic acid: A review of cell design and operation". In: *Separation and Purification Technology* 316 (2023), p. 123811. DOI: 10.1016/j.seppur.2023.123811. URL: https://doi.org/10.1016/j.seppur.2023.123811.

[13] Gamry Instruments. *Cyclic Voltammetry (CV)*. Accessed: 2025-06-10. n.d. URL: https://www.gamry.com/electrochemistry-applications/cv-cyclic-voltammetry/.

[14] Global Analyser Solutions. *CompactGC 4.0 Brochure V4 – 2018*. Accessed: 2025-06-10. 2018. URL: https://gassite.com/assets/uploads/2018/06/CompactGC4.0-brochure-V4-2018.pdf.

[15] E. A. Grinberg et al. "Electrochemical reduction of CO_2 in the presence of 1,3-butadiene using a hydrogen anode in a nonaqueous medium". In: *Russian Chemical Bulletin* 48.2 (1999), pp. 294–299. DOI: 10.1007/s11172-999-0100-1.

[16] David Harvey. *12.4: Gas Chromatography*. https://chem.libretexts.org/Bookshelves/Analytical_Chemistry/Analytical_Chemistry_2.1_(Harvey)/12:_Chromatographic_and_Electrophoretic_Methods/12.04:_Gas_Chromatography. Accessed: 2025-06-10. 2016.

[17] Gamry Instruments. *Two, Three, Four Electrode Experiments*. Accessed: 2025-04-06. 2025. URL: https://www.gamry.com/application-notes/instrumentation/two-three-four-electrode-experiments/.

[18] IPCC. *Calculating N_2O Emissions from the Production of Adipic Acid*. Accessed: 2025-04-06. Version 2.0. 2007. URL: http://www.ipcc-nggip.iges.or.jp/public/2006gl/pdf/3_Volume3/V3_3_Ch3_Chemical_Industry.pdf.

[19] Md. Nazmul Islam and Robert B. Channon. "Electrochemical Sensors". In: *Bioengineering Innovative Solutions for Cancer*. Academic Press, 2020, pp. 47–71. DOI: 10.1016/B978-0-12-813886-1.00004-8. URL: https://www.sciencedirect.com/science/article/pii/B9780128138861000048.

[20] Asvin Sajeev Kumar et al. "A Quantitative Analysis of Electrochemical CO_2 Reduction on Copper in Organic Amide and Nitrile-Based Electrolytes". In: *The Journal of Physical Chemistry C* 127.27 (2023), pp. 12857–12866. DOI: 10.1021/acs.jpcc.3c01955. URL: https://doi.org/10.1021/acs.jpcc.3c01955.

[21] Universal Lab. *Fundamentals of Electrochemical Experiments (Part 2)*. Accessed: 2025-04-06. 2025. URL: https://universallab.org/blog/blog/fundamentals_of_electrochemical_experiments_part_2/.

[22] NOAA Global Monitoring Laboratory. *Trends in Atmospheric Carbon Dioxide*. Accessed: 2025-03-31. 2025. URL: https://gml.noaa.gov/ccgg/trends/.

[23] Chuan-Hua Li et al. "Highly regioselective electrochemical synthesis of dioic acids from dienes and carbon dioxide". In: *Electrochimica Acta* 56.4 (2011), pp. 1529–1534. DOI: 10.1016/j.electacta.2010.06.057.

[24] Roman Matthessen et al. "Electrocarboxylation: towards sustainable and efficient synthesis of valuable carboxylic acids". In: *Beilstein Journal of Organic Chemistry* 10 (2014), pp. 2484–2500. DOI: 10.3762/bjoc.10.260.

[25] Measurlabs. *HPLC-DAD Analysis*. Accessed: 2025-06-10. n.d. URL: https://measurlabs.com/methods/hplc-dad-analysis/.

[26] Sayyar Muhammad and Asad Ali. "Efficient electrocatalytic reduction of CO_2 on an Ag catalyst in 1-ethyl-3-methylimidazolium ethylsulfate, with its co-catalytic role as a supporting electrolyte during the reduction in an acetonitrile medium". In: *Frontiers in Chemistry* 13 (2025), p. 1515903. DOI: 10.3389/fchem.2025.1515903. URL: https://www.frontiersin.org/articles/10.3389/fchem.2025.1515903/full.

[27] Ossila Ltd. *Cyclic Voltammetry*. Accessed: 2025-06-10. n.d. URL: https://www.ossila.com/pages/cyclic-voltammetry.

[28] Pine Research Instrumentation. *Chronopotentiometry (CP)*. Accessed: 2025-06-10. n.d. URL: https://pineresearch.com/support-article/chronopotentiometry-cp/.

[29] D. Pletcher and J. Tietje Girault. "The influence of cell design and electrolysis parameters on the cathodic coupling of butadiene and carbon dioxide in acetonitrile. I. Undivided parallel plate configurations". In: *Journal of Applied Electrochemistry* 16.6 (1986), pp. 791–802. DOI: 10.1007/BF01006524.

[30] Ch. V. V. Ramana et al. "Dielectric and Excess Dielectric Constants". In: *Journal of Chemistry* 2013 (2013), pp. 1–4. DOI: 10.1155/2013/687106. URL: https://doi.org/10.1155/2013/687106.

[31] Sigma-Aldrich. *1,3-Butadiene solution*. Product No. 695580, Accessed: 2025-06-10. n.d. URL: https://www.sigmaaldrich.com/NL/en/product/aldrich/695580.

[32] American Chemical Society. *Adipic Acid*. Accessed: 2025-04-06. 2015. URL: https://www.acs.org/molecule-of-the-week/archive/a/adipic-acid.html.

[33] Stephan N. Steinmann et al. “Electro-carboxylation of butadiene and ethene over Pt and Ni catalysts”. In: *Journal of Catalysis* 343 (2016), pp. 240–247. DOI: 10.1016/j.jcat.2016.01.008.

[34] Technobis Crystallization Systems. *Crystal16®*. Accessed: 2025-06-10. n.d. URL: https://www.crystallizationsystems.com/products/crystal16/.

[35] Technobis Crystallization Systems. *Solubility Applications*. Accessed: 2025-06-10. n.d. URL: https://www.crystallizationsystems.com/applications/solubility/.

[36] Applicant(s) Unknown. “Electrocarboxylation of 1,3-Butadiene”. US00000011913127B2. 2020. URL: https://patents.google.com/patent/US00000011913127B2/en.

[37] Verulam Scientific. *CompactGC 4.0*. Accessed: 2025-06-10. n.d. URL: https://verulamscientific.com/gas-compactgc4-0/.

[38] Stijn Van de Vyver and Yuriy Roma´n-Leshkov. “Emerging catalytic processes for the production of adipic acid”. In: *Catalysis and Science Technology* Volume Number (2012), pp. 1465–1479. DOI: DOI:10.1039/c3cy20728e.

[39] Waters Corporation. *Identifying and Quantitating Compounds*. Accessed: 2025-06-10. n.d. URL: https://www.waters.com/nextgen/nl/en/education/primers/beginner-s-guide-to-liquid-chromatography/identifying-and-quantitating-compounds.html.

[40] Charles R. Campbell Werner H. Mueller and John J. Hicks Jr. “Process of preparing adipic acid by the nitric acid oxidation of cyclohexane”. 3654355 (St. Louis, Mo.). Apr. 1972. URL: https://patents.google.com/patent/US3654355A/en.

[41] Gao-Qing Yuan et al. “Efficient electrochemical synthesis of 2-arylsuccinic acids from CO_2 and aryl-substituted alkenes with nickel as the cathode”. In: *Electrochimica Acta* 53.6 (2008), pp. 2170–2176. DOI: 10.1016/j.electacta.2007.09.023.

[42] Mi Zhang et al. “Mechanism of efficient electroreduction of CO_2 to CO at Ag electrode in imidazolium-based ionic liquids/acetonitrile solution”. In: *Applied Catalysis B: Environmental and Energy* 359 (2024), p. 124508. DOI: 10.1016/j.apcatb.2024.124508.

A

Appendix

A.1. Statistics and Data Processing

Area of the HPC peaks, depending on the retention time of the product peaks at their elution times, is noted. A couple of injections per vial are analysed for increased accuracy in the calculation of the area of the peak. The accurate area of the peak is calculated by taking the average of the two values of peak areas.

$$Area(HPLC) = \frac{(Area_1 + Area_2)}{2}$$

$$concentration(mM) = \frac{(Area(HPLC) - b)}{a}$$

where a and b are the calibration line intercepts with a regression of more than 99%. The equation of the line is $y = a \cdot x + b$. These calibration curves are plotted with the equation lines and are reported in the Appendix A.2.

$$3HDA : y = 9260.8 \cdot x + 134.92, R^2 = 0.9999$$

$$3PA : y = 6368.6 \cdot x + 232.91, R^2 = 0.9996$$

$$Formate : y = 1438.1 \cdot x + 20.23, R^2 = 0.9999$$

$$OA : y = 7678.9 \cdot x - 390.01, R^2 = 0.9999$$

The next set of equations determines the amount of product in milligrams in the HPLC sample.

$$concentration(mmol/ml) = \frac{concentration(mM)}{1000}$$

$$concentration(mg/ml) = concentration(mmol/ml) \cdot mol.wt$$

Molecular weights of the products are as follows: 3HDA = 144.13 g/mol, 3PA = 100.12 g/mol, Formate = 45.017 g/mol, and oxalic acid = 90.03 g/mol.

$$concentration(mg) = concentration(mg/ml) \cdot volume(ml)$$

Here, the concentration in mg is the weight of 3HDA in the HPLC sample. where volume is taken as the HPLC vial volume. Usually, 1.5 ml of sample is made by the addition of 5 mM $H2SO4$ and 0.5 M NaOH.

$$\%selectivity = \frac{concentration(mg)}{weight_{sample}(mg)} \cdot 100$$

where the weight of the sample in mg is the amount of solid sample taken in the vial from the collected sample, after drying the centrifuged solid counterpart.

$$Product = \%selectivity \cdot weight_{collected}(mg)$$

Product is the total amount of 3HDA within from the total solid sample collected. For calculating the final amount of product formed, the time for completion of the reaction, i.e the time taken to convert all of the 1,3-butadiene, needs to be calculated. The concentration of 1,3-butadiene in the electrolyte solution is 150 mM, in a 40 ml system, making it 6 millimoles of 1,3-butadiene, as 1,3-butadiene is a raw material in 20% v/v toluene [31].

$$Q_{1,3-butadiene} = 0.006 \cdot n \cdot F(C)$$

Where $Q_{1,3-butadiene}$ is the charge taken for the complete conversion of 1,3-butadiene, 'n' is the number of electrons per molecule and 'F' is the Faraday's constant, i.e 96485 C/mol.

$$time = \frac{Q_{1,3-butadiene} \cdot 1000}{I \cdot 3600}(hr)$$

Where current (I) is in mA and 3600 is seconds per hour. 'time' is the time required for the reaction to complete. Once the time is calculated, the multiplication factor (MF) is calculated.

$$MF = \frac{time(hr)}{2(hr)}$$

Since the chronoamperometry experiment is run for 2 hours, the MF is calculated for the number of times the 2-hour experiment needs to be extrapolated to find the expected amount of product on completion of the reaction.

$$FinalProduct = Product \cdot MF(mg)$$

The ideal amount of product formed is when all the 6 millimoles of 1,3-butadiene are converted to the desired product.

$$Ideal_{amount} = moles \cdot mol.wt(mg)$$

Having the ideal amount of product and the expected final product allows the calculation of the product yield percentage and the isolated yield percentage. Isolated yield percentage is the ratio of the product formed after its selectivity is considered among the solid sample.

$$\%yield = \frac{FinalProduct(mg)}{Ideal_{amount}(mg)} \cdot 100(\%)$$

$$\%isolated.yield = \frac{FinalProduct(mg)}{Ideal_{amount} \cdot \%selectivity(mg)} \cdot 100(\%)$$

For the faradaic efficiency calculation, the amount of charge taken by the product needs to be considered.

$$Q_{product} = N \cdot n \cdot F(C)$$

Where $Q_{product}$ is the charge taken for the formation of the product, 'n' is the number of electrons per molecule of the formed product and 'F' is the Faraday's constant, i.e 96485 C/mol. 'N' is the number of moles of product formed and is calculated by Equation A.1.

$$N = \frac{V \cdot Area(HPLC)}{1000}(mol)$$

Where V is the volume of the electrolyte, that is, 40 ml. The faradaic efficiency is thus calculated as,

$$\%FE = \frac{Q_{product}(C)}{Q_{taken}(C)} \cdot 100(\%)$$

Where Q_{taken} is a value from the graph of ECLab, calculated on the dynamic basis of the current flowing for the 2-hour duration of the reaction.

A.2. HPLC Calibration Curves

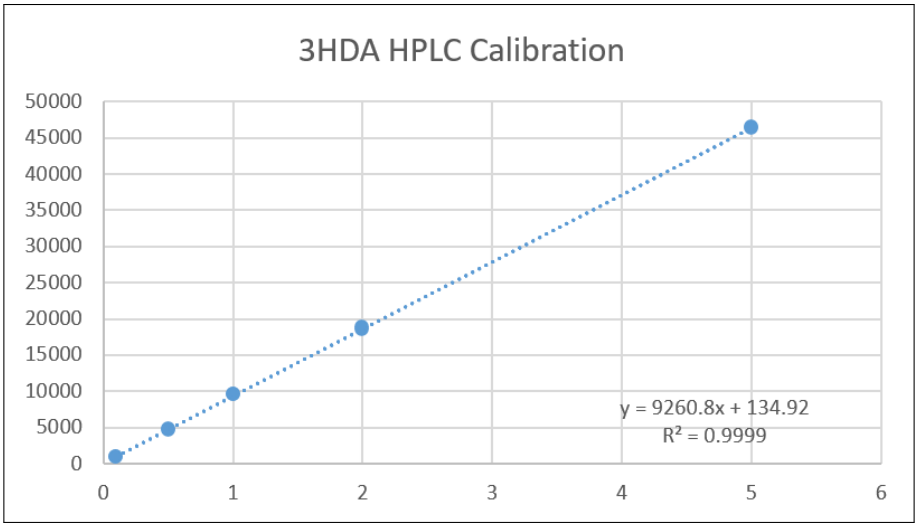

Figure A.1: 3HDA HPLC Calibration Curve

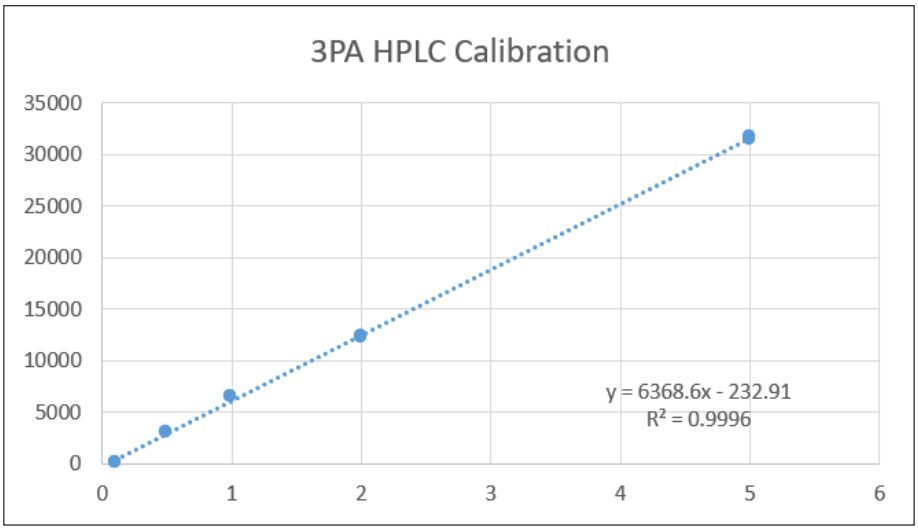

Figure A.2: 3PA HPLC Calibration Curve

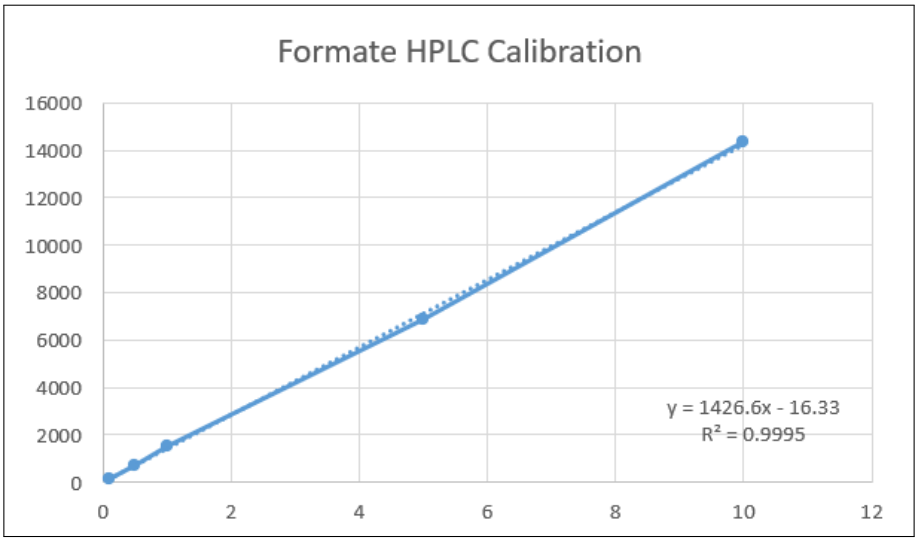

Figure A.3: Formate HPLC Calibration Curve

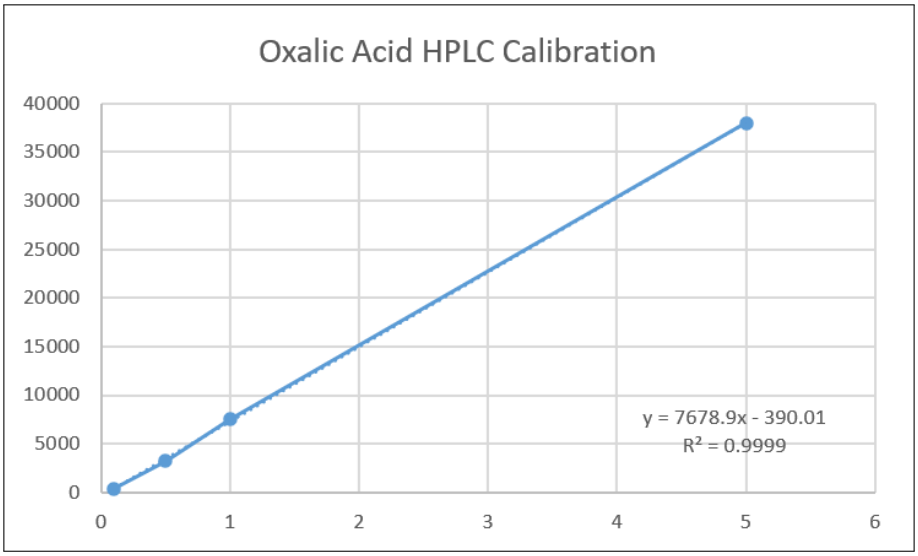

Figure A.4: Oxalic Acid HPLC Calibration Curve

A.3. Liquid GC Calibration Curves

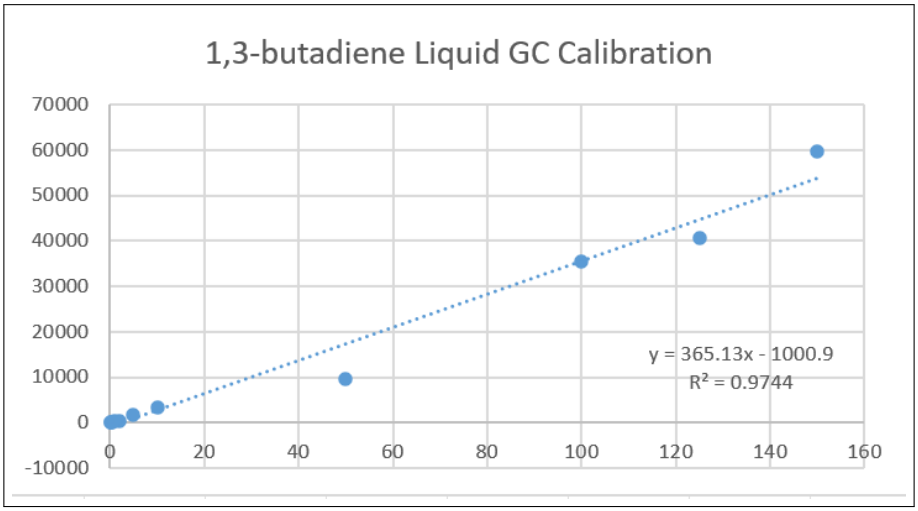

Figure A.5: 1,3-butadiene Liquid GC Calibration Curve

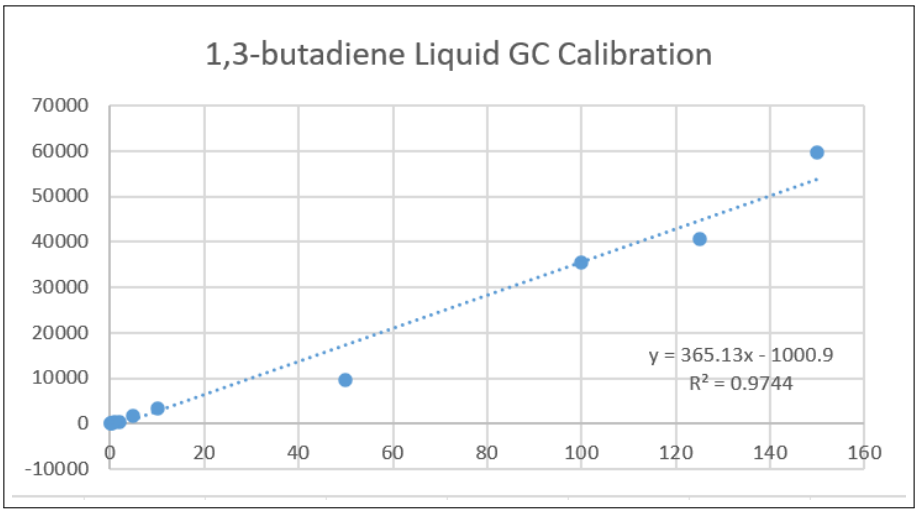

Figure A.6: 3PA Liquid GC Calibration Curve

A.4. Scanning Electron Microscopy

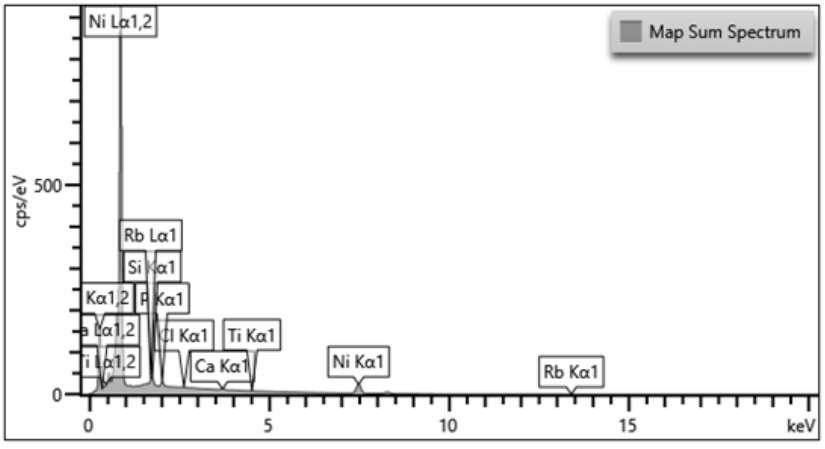

Map Sum Spectrum

Element	Signal	Weight %
Ni	81.65	0.06
C	15.92	0.05
Rb	0.99	0.02
P	0.54	0.01
Si	0.46	0.01
Ca	0.29	0.01
Cl	0.07	0.01
Ti	0.07	0.01

Figure A.7: Nickel wire SEM map and spectrum signal used in acetonitrile and $TBAPF_6$ electrolyte solution